BACHELOR THESIS

SKIM MILK DRYING IN A LAB-SCALE COUNTER FLOW SPRAY DRYER

Ilambharathi G
S2467259
EXCHANGE STUDENT

FACULTY OF ENGINEERING TECHNOLOGY
DEPARTMENT OF THERMAL AND FLUID ENGINEERING
UNIVERSITY OF TWENTE

EXAMINATION COMMITTEE
Dr.ir.A.K.Pozarlik
U. Jamil Ur Rahman

SUMMARY

Milk powder is a significant dairy product which is useful in transportation and preservation of milk. It is used as a nutrient rich food as well as saturating agent. The milk powder is produced by drying the concentrated liquid milk. However, the current drying methods are energy intensive and also suffer from wall deposition of particles. So, improving energy efficiency and reducing deposition is inevitable. In industries, milk powder production is mainly carried out by spray drying in a co-current flow. The RMZD project aims to achieve high evaporation in a small reactor. Therefore, high temperatures are employed by using a counter-flow setup. This thesis focuses on the experimental study of milk spray drying and development of CFD model to predict the drying along with corresponding wall deposition.

The counter flow spray drying is investigated with a lab scale test reactor. Water feed is initially used in order to obtain the favorable process conditions for spray drying of skim milk. Thereafter, milk feed is used in the reactor to observe the temperature profiles, particle yield and deposition patterns. The temperature profiles depend on the water content and deposition is mainly due to sugars present in the milk, above the glass transition temperature. It has been observed that, for the particular process conditions most particles stick inside the reactor and a small portion reaches the cyclone.

A CFD model is developed for the same reactor. The temperature drop in hot air flow is incorporated through heat loss model and validated against the experimental results. The droplet diameters in the break up region are used to model the diameter distribution of the droplets. Drying model for water is developed and a close similarity is found with experimental results. This model is extended with multicomponent case to further model the drying of skim milk, but the drying rate in reality is hindered by the kinetics. Therefore reaction engineering approach (REA) is used to model the drying kinetics.

The single droplet - drying experiments from the literature is used to validate the REA model. Then it is incorporated in the spray drying case in order to accurately model the evaporation rate. Spray drying of milk is validated in good agreement with the experimental data. The average errors are found to be 5%, 32% and 26% for air only, water and skim milk cases respectively. Deposition of particles along the wall is modeled based on the sticky point temperature. The CFD results are qualitatively validated with the experimental results.

CONTENTS

1.INTRODUCTION **1**

1.1 Background 1

1.2 Aim of the study 1

2.LITERATURE REVIEW **2**

2.1 Components of spray drying process 2

2.2 Experimental Research 4

2.3 CFD model 4

2.4 Drying model 5

2.4.1 REA model 5

2.5 Deposition model 6

3. METHODOLOGY 6

3.1 CFD Methodology 6

3.1.1 Governing equations - continuous phase 6

3.1.2 Turbulence model 7

3.1.3 Eulerian- Lagrangian Approach 7

3.1.4 Governing equations - discrete phase 8

3.1.5 Drying model 9

3.1.6 Numerical strategy 11

3.1.7 Deposition model 11

3.1.8 Geometry and boundary conditions 11

3.2 Experimental Methodology 14

4. RESULTS AND DISCUSSION.....15

4.1 Experimental results.....15

4.1.1 Experiment - Air only.....15

4.1.2 Experiment - water.....16

4.1.3 Experiment - milk.....17

4.2 CFD results.....20

4.2.1 Single droplet drying.....20

4.2.2 Heat loss model.....20

4.2.3 Water drying model.....22

4.2.3 Milk drying model.....25

4.2.4 Wall deposition model.....29

5. CONCLUSIONS AND RECOMMENDATIONS.....34

REFERENCES.....35

APPENDIX.....38

A. Mesh Independence study.....38

B. Droplet size data.....39

C. Nozzle calibration.....40

D. UDFs.....41

E. Cross sectional comparison of temperature profiles.....49

1. INTRODUCTION

1.1 Background

While the world countries are focusing on economic growth and sustainable development, it is inevitable to intensify the industrial processes by technologies which are cleaner, miniaturized, energy efficient and cost effective. Drying is usually applied to make a durable product that is easy to handle and, after reconstitution with water, has similar properties to the original material. However, drying is a highly energy intensive unit operation contributing to approximately 12% of the total energy consumption in industrial sectors [1]. One of the most important dried products is milk powder. It is a major part of relief supplies in times of war and natural disasters as it is easily transportable and can provide high content of nutrients. It is also tailored to the regular needs of consumers by varying the nutrient content and flavor. The widely used process of milk powder production is spray drying.

Spray drying is a process in which liquid feed is converted into dry powder using a gas medium. Among available methods of drying, spray drying is preferred over drum drying and freeze drying, due to its continuous process method , reduced cost, shorter drying time, effective drying and higher moisture removal rate [2, 3]. It provides control over particle size, bulk density and degree of crystallinity [4]. It is also used to produce other food products such as whey protein, coffee, instant soup as well as detergents, pesticides and antibiotics [5]. The major advantages of spray dried products are longer shelf life, low transportation costs and novel products. Conventional spray dryers operate at low temperatures as the particle residence times are longer due to the large size of the dryer. In addition to high energy consumption, drying sugar rich materials like milk suffers a major issue of powder deposition along the dryer walls, leading to low product quality, difficult powder recovery and clogging of nozzles. In order to address these issues, the Radial-Multizone dryer (RMZD) project was started. The RMZD intensifies spray drying in a relatively small reactor by offsetting low residence time with high temperature counter flow, leading to low specific energy consumption. It uses mild temperature tangential vortex flow in the along the periphery of the reactor to separate the powder effectively with improved product quality [6].

1.2 Aim of the study

This study focuses on counter flow spray drying of milk. Optimization of spray drying requires a clear understanding of the process inside the reactor. But the complexity of process, involving transport phenomena, multiphase turbulent flow and material properties make it difficult to understand, especially with the particle deposition. Each experiment with milk in the test reactor consumes a large amount of time in disassembling and cleaning the reactor. Therefore the focus of this study is to develop and validate a CFD model for the counter flow test reactor. The specific focus are

1. Conduct experiments in the lab-scale reactor with water and skim milk.
2. Develop a CFD model for counter flow test reactor
3. Validate the heat loss, drying of water and skim milk with experimental results
4. Incorporate Reaction Engineering Approach (REA) based mass transfer and validate with experimental data from the literature
5. Compare REA with default Raoult's law based approach for mass transfer in FLUENT
6. Qualitatively analyze the wall deposition of sticky particles based on sticky point temperature

2. LITERATURE REVIEW

In spray drying, the liquid feed containing dissolved solids, is dehydrated by transforming the mixture into spray of small droplets and exposing them to hot air. The large surface area of the droplets causes evaporation of the water to take place efficiently. The two basic types of spray dryer are short-form and tall-form designs. The tall form designs have diameter ratio greater than 5:1 [7]. The major components of the setup are hot air system, feed system, atomizer, drying chamber and particle separation system. The most important steps of spray drying are atomization, droplet-air contact and droplet drying.

2.1 Components of spray drying process

Atomizer or spray nozzle is used to disperse the liquid or slurry into a controlled drop size. The atomization stage is the most important step in the spray drying process creating the optimum conditions for evaporation of liquid droplets into dried product with specific characteristics. The commonest atomizers are rotary disks and single-fluid pressure swirl nozzles. Two-fluid and ultrasonic nozzles are also used, however only in lab scale reactors[4]. In industries, pressure nozzles are preferred over others as the pump for creating the high slurry pressures needs lesser energy than the compressed gas and result in particles with less occluded air producing powders of higher density, with good flow characteristics [5]. Liquid is pressurized by a pump and forced through an orifice to break the liquid into fine droplets, therefore pressure and velocity are coupled in droplets. Higher the feed viscosity, more atomizing energy is required for smaller droplets.

There are various spray patterns such as flat fan, full-cone and hollow cone[8]. The slurry flows through the swirl chamber inside the nozzle and disintegrates into droplets. Among the spray patterns, hollow cone provides the smallest droplet sizes leading to efficient evaporation [9]. The aim of atomizing the concentrate is to provide a very large surface, from which the evaporation can take place. The smaller droplets, the bigger surface, the easier evaporation, and a better thermal efficiency of the dryer are obtained. The ideal condition would be a spray of same droplet size, as the drying time for all particles would be the same for obtaining equal moisture content [10]. The angle of spray also influences drying and it generally is based on the type of flow. A wider angle of spray is used with the co-current flow as the downward-flowing air narrows down the spray angle and with the counter-current flow a narrow angle is used since the spray moving downward is widened by the upward-flowing air [5].

When droplets contact with hot gas, moisture evaporates rapidly from the droplet surface. When the spray comes in contact with the air, the droplets usually meet air in either co-current or counter current manner. In co-current flow, spray flows in the same direction as that of hot air resulting in low residence time of particles compared to counter current flow. In counter-current flow, spray flows in the opposite direction as that of hot air. It maintains a nearly constant gradient between the two flows over their entire length of contact, resulting in better heat and mass transfer. In mixed flow, feed moves in opposite direction as in counter flow, whereas product moves in the same direction of outlet gas resulting in maximum residence time of particles compared to other flows [4, 11]. In co-current flows involving heat sensitive materials, low inlet temperatures are used, since droplet residence times in such dryers are much longer [12, 13].

In drying, both free moisture and internal moisture are removed. When the feed is introduced into hot air, temperature rises to the wet bulb temperature. Evaporation of moisture comprises of constant rate period and falling rate period (see Fig.1). Moisture evaporation occurs at a constant rate in wet bulb temperature until a critical value of the droplet water content is reached and a thin shell (also known as crust/skin) is formed at the droplet surface [9]. In the falling rate period, the liquid leaving the solid decreases and the drying is diffusion rate limited. The liquid that is trapped inside the particles diffuses to the outside surface of the particle through capillary action [14].

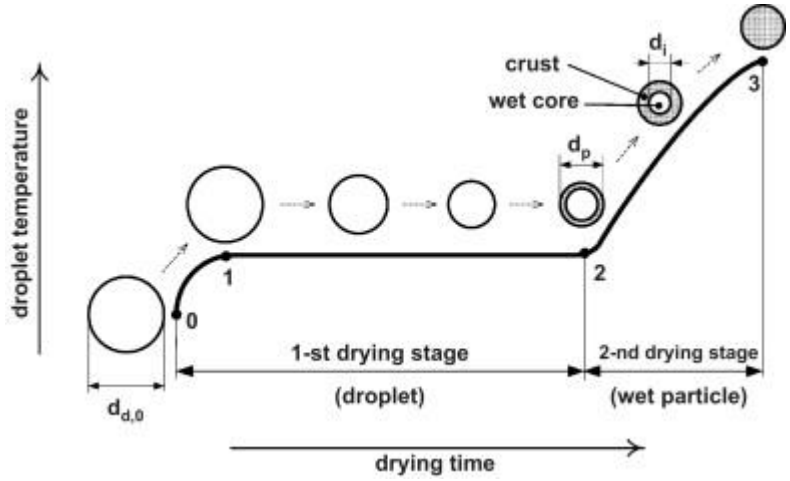

Fig.1 Droplet drying [15]

Agglomeration is the adherence of smaller particles to each other to form powder. It mainly occurs due to droplet-droplet interaction near nozzle and particle-droplet interaction due to venture effect. Other than these, particles also deposit at the wall surface, when high velocity droplets contact directly with dried particles close to the wall [16, 17]. This adhesion of powder particles with the walls of drying chamber is the main cause for material loss in spray drying of sugar and acid rich foods. Powder stickiness is a cohesion-adhesion property. It can be explained in terms particle–particle stickiness (cohesion) and particle–wall surface stickiness (adhesion). In milk, it is mainly due to presence of low molecular weight sugar, lactose. The high hygroscopicity, relative humidity, thermoplasticity, molecular mobility due to reduced viscosity on heating and low glass transition temperature (Tg) contribute to the stickiness problem [18, 19].

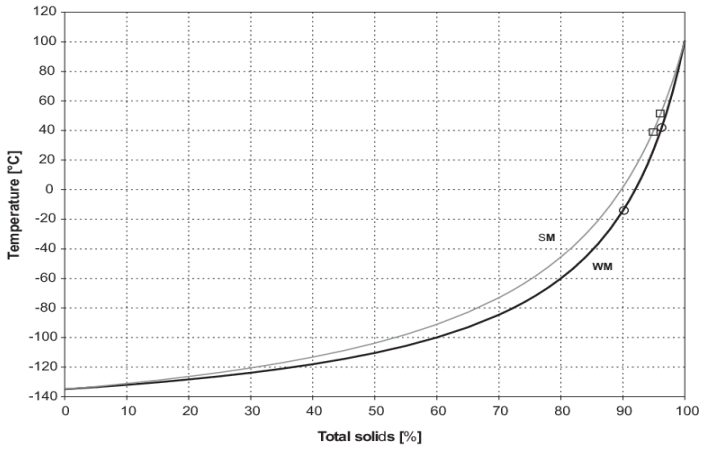

Fig.2 Tg lines of Whole Milk (WM) and Skim Milk (SM) according to the Gordon-Taylor equation [20]

Stickiness issue is controlled through material and/or process approaches. In material based approach glass transition temperature is increased with high molecular weight additives. The most commonly used additives used in spray drying include maltodextrins, gum arabic and starch due to their high solubility and less viscosity. While in process approach, cooling the walls of dryer chamber, swirling inlet flow, low humidity and low drying temperature can be used to reduce wall deposition. Depending on method of separation, it is classified into single-stage, 2-stage and 3-stage drying. The most used separators in the milk powder industry are cyclone, bag filter and wet scrubber [17].

2.2 Experimental research

Birchal et al. [21] concluded that the properties of milk powder depend on the process parameters such as feed flow rate, air flow rate and inlet air temperature. Rao et al. [22] estimated that the relative yield of powders increase with total solids as there will be lesser water to evaporate. Martens et al. [23] showed that, at constant feed rate and nozzle pressure, the droplet size increases with increase in viscosity, which in turn reduces the effective surface area resulting in improper drying. A research conducted by Piatkowski et al. [24], estimates that in counter flow spray dryers, as the distance of nozzle position from the air inlet increases, the temperature in agglomeration zone decreases. It is noted that agglomeration is poor at higher temperatures. Cheng et al. [25] showed that thermal efficiency of dryer can be increased by increasing the inlet air temperature and feed temperature, but limited by product nature especially in counter flow configuration. Telang et al. [26] found that, although yield increases with inlet temperature, beyond the glass transition temperature decreases due to sticking. Francia et al. [16] performed a study on detergent drying in counter flow dryer, the authors concluded, when nozzle is positioned close to air inlet, the residence time reduces forming coarse particles with reduced efficiency. But the top location of counter flow, promotes elutriation and wide particle size distribution. Therefore an optimum location is far from the top to allow the fine powder to migrate to the walls and away from the bottom to maintain a sufficient residence time for the product to dry. The overall performance of a dryer is estimated by the difference between inlet and outlet temperatures, specific energy consumption, wall deposition and evaporation rate [1].

2.3 CFD model

Computational Fluid Dynamics (CFD) provides a major advantage of predicting the influence of process parameters, particle agglomeration and tracking without much of capital investments and time consumption. Many studies have been done in spray drying modeling by using CFD. Although many authors have used 2D axisymmetric models for spray drying models in the past, Mezhericher et al. [27] reported that 3D models predict asymmetry of flow patterns, transversal air flow and provide actual 3D representation of particle trajectories leading to better accuracy of results. Crowe et al. [28] used particle source in cell (PSI-cell) with CFD to model spray drying. This is the basis for the discrete phase model (DPM) which is used by most of the authors now. This concept treats the gas as a continuum phase (Eulerian) and the spray as a discrete tracked phase (Lagrangian). Kieviet et al. [29] concluded that air flow patterns, temperature and humidity profiles of experimental results agreed well with the CFD results inside the drying chamber. Langrish et al. [30] studied the effects of inlet geometry and spray angle in wall deposition using numerical simulation. Huang et al. [31] used CFD model with different geometries and concluded that there are significant differences in particle trajectories and residence times within different geometry chambers. In another study by Huang et

al. [32], they compared the effects of rotary disc atomizer and pressure nozzle in a co-current spray dryer with maltodextrin feed using CFD by concluding that deposition patterns are highly dependent on the type of atomizer. They also found that pressure nozzle may lead to a high velocity variation with high recirculation in the center of the chamber than the rotary atomizer. Nijdam et al. [33] concluded that the Lagrangian approach gives a good prediction for modeling droplet evaporation. Drying multicomponent droplets is hindered by drying kinetics, so the kinetics is included before modeling wall deposition. Tran et al. [34] developed a CFD model based on characteristic drying curve and validated with experimental results, by comparing moisture content of the particle at different heights of a co-current spray dryer. Huang et al. and Anandharamakrishnan et al. [35, 36] validated their CFD models for milk with experimental data based on temperature and moisture at different axial and radial positions inside the drying chamber. Similarly, Maryam et al. [37] used axial and radial temperature profiles to validate their CFD study on skim milk and salt solution with 10% total solids.

2.4 Drying model

Modeling stickiness requires accurate temperature and moisture near wall, therefore incorporation of drying kinetics is necessary. The following drying models are mainly reported in the literature. In internal moisture diffusion approach, internal moisture transfer by molecular diffusion and species convection is taken into account [38]. In receding interface approach, internal conduction and external convection resistances control the drying rate [39-41], but both of these approaches are computationally expensive and requires experimental evaluation of moisture diffusivity [42].The characteristic drying curve approach (CDRC) and reaction engineering approach (REA) consider the particles as lumped mass in which the average properties are taken for the particle. In CDRC approach, the relative drying rate is directly proportional to the free moisture content, and requires separate modeling for constant and falling drying rate [43]. Patel et al. [44] compared CDRC and REA approaches by CFD simulations and concluded that CDRC approach fails at high concentration, high humidity conditions, whereas REA approach predict more realistically including the droplet trajectories with a relatively simple approach. REA is preferred to model the drying kinetics.

2.4.1 REA model

Chen et al. [45] introduced REA approach which considers drying as a competitive process between evaporation and condensation. The relationship between activation energy and moisture content is taken as the fingerprint of the process, the energy barrier increases with decrease in moisture content, but the very initial time period is not taken into account. In a further study by Chen et al. [46] about single milk droplet drying in air, the REA model was modified for better predictions based on experimental data and concluded that CFD results are close to experimental results. Pawar et al. [47] modeled similar conditions to validate the model and incorporated to a large scale spray dryer. They concluded that the droplet size during drying does not match with experimental results due to shrinking to non-spherical shapes.

In a critical review of REA model by Chen et al. [48], it is reported that the drying curve of activation energy varies with initial concentration and appropriate fitting constants should be included. It also describes the relationship between CDRC and REA approaches. In a research by Fu et al. [49], it is concluded that the activation energy curve remain similar for different droplet diameters with same initial concentration, but the initial droplet diameter influences the heat-mass transfer

coefficients, surface area and crust formation phenomena, so it proposes a linear, polynomial master curve correlations for diameter changes with respect to free moisture content. Jin et al. [50] numerically modeled a transient two-dimensional axisymmetric multiphase and multi-species flow in Eulerian - Lagrangian approach for drying with REA model through UDF in Ansys FLUENT. The authors found that medium-size particles are found near the side walls rather than dense particle clouds. In a further study by Jin et al. [51], a 3D transient case in Eulerian - Lagrangian approach with REA model was simulated and they found a close prediction of temperatures at wall when compared with experimental data.

2.5 Deposition model

The explanations for discrete phase boundary conditions (ESCAPE and REFLECT) can be found in ANSYS Fluent manual [52]. In the earlier works, the droplets were often assumed to penetrate the wall as soon as they touched the wall surface by using ESCAPE boundary condition with either one way or two way coupling [35, 53]. But they do not represent the deposition realistically and also affects the accuracy of continuous phase solutions. Jin et al. [50] concluded that REFLECT wall boundary condition produced more physically correct results for normal dryer operation than ESCAPE. Kota et al. used deposition co-relation for pipe flows to model wall deposition but they concluded that it provided results with significant deviation [54]. It has been well understood that stickiness depends strongly on the glass transition temperature. The sticky behavior of sugar rich components is observed 23.3°C above glass transition temperature [55]. Harvie et al. [56] developed a model for wall deposition based on the sticky point temperature by altering the co-efficient of restitution during the wall impact. Jin et al. [57] incorporated the droplet-wall film approach by classifying the droplet as surface tension–dominated droplet, viscous force-dominated droplet and dry particle. Their impact with film wall and dry wall was used to model wall deposition. But this approach requires effective modeling of wall films and droplet-wall film interaction.

3. METHODOLOGY

3.1 CFD methodology

The commercial CFD software Fluent 19.3 was used for simulation. A steady state, three dimensional case is considered to be solved. Spray drying involves multiphase, multi species, turbulent flow with heat and mass transfer.

3.1.1 Governing equations - continuous phase

The following equations govern the gas phase. The continuity equation is given by,

$$\frac{\partial \rho}{\partial t} + \nabla \cdot (\rho \vec{v}) = S_m$$

Where ρ is the gas density, $\vec{v}$ is the gas velocity and S_m is the mass source term

Momentum equation is given by,

$$\frac{\partial (\rho \vec{v})}{\partial t} + \nabla \cdot (\rho \vec{v} \vec{v}) = -\nabla P + \nabla \cdot (\tau) + \rho \vec{g} + \overrightarrow{S_f}$$

Where P is the static pressure, τ is the stress tensor, $\rho \vec{g}$ is the gravitational body force, $\overrightarrow{S_f}$ is the body force that arises from interaction with the dispersed phase.

The stress tensor is given by,

$$\tau = \mu[(\nabla \vec{v} + \nabla \vec{v}^{\,T}) - \frac{2}{3} \nabla \cdot \vec{v} I]$$

Where μ is the molecular viscosity, I is the unit tensor.

Energy equation is given by,

$$\frac{\partial (\rho E)}{\partial t} + \nabla \cdot (\vec{v}(\rho E + P)) = \nabla \cdot (k_{eff} \nabla T - \sum_j h_j \overrightarrow{J_j} + (\tau_{eff} \cdot \vec{v})) + S_h$$

Where T is the temperature, E is the total energy, k_{eff} is the effective thermal conductivity including turbulent thermal conductivity, h_j is the sensible enthalpy of species j and $\overrightarrow{J_j}$ is the diffusion flux of species j and S_h is the volumetric heat source.

3.1.2 Turbulence model

During spray drying the particle behavior is dependent on the air flow pattern. Therefore, modeling the turbulent flow properly is inevitable. The most commonly used turbulence models for spray drying in increasing order of computational expense are standard k–ε, RNG k–ε, SST k – ω of Reynolds averaged Navier stokes (RANS) framework and Reynolds Stress Model (RSM) [58, 59]. K – ε model gives better predictions for far-wall free shear flows and k – ω for near-wall flows [60]. k – ω SST model solves well for both near and far wall regions, but k–ε model with wall functions can be used to model both regions in a much lower computational expense with a relatable accuracy for non-

swirling flows. Hasan et al. [58] concluded that k – ω SST predicts slightly better of dissipation of hot air jet over k- ε models. However authors have concluded that standard k–ε provides better results for non-swirling flows whereas RNG k–ε, RSM solves better for highly swirling flows [61, 62]. Huang et al. [63] concluded that a 3D CFD model gave close results with experimental data with use of standard k–ε model. Since the model for this study is relatively simple with no significant swirls, standard k–ε model based on transport of turbulent kinetic energy (k) and rate of its dissipation (ε) is used. Therefore heat transfer through the wall requires proper modeling of near wall. But the highly variable local velocities throughout the chamber near wall make it difficult to maintain the wall y+ values in ranges, so the scalable wall function is used. It ensures that the wall distance employed in the wall functions is such that $y^+ \geq 11.1$ irrespective of the level of near-wall grid refinement. It forces the usage of the log law in conjunction with the standard wall functions approach. The governing equations of standard k–ε model and scalable wall function can be found in ANSYS Fluent theory guide [64, 65].

3.1.3 Eulerian- Lagrangian Approach

The two methods commonly used to model multi-phase flows are Eulerian-Eulerian and Eulerian - Lagrangian methods. Eulerian-Eulerian method treats each phase as a continuum, it is appropriate when the two phases are at similar fractions. But the droplets in spray drying occupies very small portion of the volume. In a spray dryer, where the volume fraction of droplet phase is less than 10%, Eulerian - Lagrangian approach is preferred. It is based on tracking individual parcels in cells of the continuous domain by using Discrete Phase Model (DPM). DPM does not consider individual particles but as parcels, based on number of parcels and feed flow rate. In this case 10 parcels are used to model the discrete phase. Hollow cone pressure nozzle atomization model is used in this study. The most important parameter in modeling spray drying is the droplet diameter. It determines mass and surface area of the droplet, which significantly influences the momentum, heat and mass transfer. Therefore experimental data for particle diameter based on different pressures at the primary break up region of spray is used and can be found in the appendix. They are extrapolated for higher pressures. Primary breakup is the region where the liquid jet or sheet interact with the gas-phase and break-up into drops of different sizes. Rosin-Rammler distribution is used to calculate the particle diameter distribution based on Sauter Mean Diameter (SMD), D90 and D10 values, with 3.5 as the spread parameter. Stochastic particle tracking is used solving 10 different possible paths, so that average path is estimated. Two way coupling is enabled so that momentum, heat and mass are transferred between continuous and discrete phase.

3.1.4 Governing equations - discrete phase

The governing equations for droplet/particle are as follows,

The particle force balance is given by the sum of drag forces, body forces and gravitational forces,

$$\frac{du_p}{dt} = F_D(u - u_p) + \frac{g_x(\rho_p - \rho)}{\rho_p} + F_x$$

Where F_D is the drag force per unit mass, u is the fluid velocity, ρ is the density of fluid, F_x is the other explicitly defined body forces for particle, u_p is the particle velocity and ρ_p is the particle density, g_x is the gravitational acceleration. Drag force is given by,

$$F_D = \frac{18\mu}{\rho_p d_p^2}\frac{C_D Re}{24}$$

Where d_p is the particle/droplet diameter, Re is the relative Reynolds number based on relative velocity between particle/droplet and gas, C_D is the drag co-efficient calculated based on Re by spherical drag law. The change in temperature for a particle is given by the equation,

$$m_p c_p \left(\frac{dT_p}{dt}\right) = hA_p(T_b - T_p) + \sum_i \frac{dm_i}{dt} h_{fg}$$

Where T_p is the particle temperature, T_b is the gas/bulk phase temperature, i is the specie, m_p is the particle mass and h_{fg} is the latent heat of vaporization. In our case, water is the only evaporating species. Therefore i is water in particle.

The heat transfer co-efficient is calculated using Ranz-Marshall equation that relates Prandtl number with Nusselt number. The mass transfer from the droplet is defined by the equation,

$$\frac{dm_p}{dt} = h_m A_p(\rho_{v,surf} - \rho_{v,b})$$

Where $\rho_{v,surf}$ is the surface vapor concentration, $\rho_{v,b}$ is the bulk vapor concentration , A_p is the surface area of the particle, h_m is the mass transfer co-efficient. Bulk vapor concentration is calculated by

$$\rho_{v,b} = \phi_{w,b}\frac{P}{RT_b}$$

Where $\phi_{w,b}$ is the mole fraction of water in air, P is the pressure, R is the Universal gas constant and T_b is the gas temperature. In Raoult's law based approach, $\rho_{v,surf}$ is calculated by

$$\rho_{v,surf} = \phi_w \frac{P_{sat}}{RT_p}$$

Where ϕ_w is the mole fraction of water in particle, P_{sat} is the saturation pressure and T_p is the particle temperature. Mass transfer co-efficient is calculated using Sherwood number co-relation,

$$Sh = \frac{h_m d_p}{D_{air-vapor}} = 2.0 + 0.6 Re_d^{1/2} Sc^{1/3}, \quad Sc = \frac{\mu}{\rho D_{air-vapor}}$$

Where Sc is the Schmidt number, d_p is the particle/ droplet diameter, $D_{air-vapor}$ is the diffusivity of vapor to air, Re_d is the Reynolds number of droplet, μ is the viscosity of air-vapor mixture and ρ is the density of air vapor mixture. In two way coupling, mass, momentum and heat transfer of discrete phase interact with gas phase through the source terms S_m, $\vec{S}_f$ and S_h respectively

3.1.5 Drying model

The Reaction Engineering Approach is incorporated by modifying particle/ droplet surface vapor concentration based on apparent activation energy of drying, which indicates higher energy needed to remove the water as the moisture content goes low.

$$\rho_{v,surf} = \rho_{sat} \times exp\left(\frac{-\Delta E_v}{RT_p}\right)$$

Where ρ_{sat} is the saturation concentration, which is calculated based on average surface temperature, ΔE_v is the apparent activation energy. Saturation concentration is calculated using correlation [66].

$$\rho_{sat} = 4.844 \times 10^{-9}(T_p - 273)^4 - 1.4807 \times 10^{-7}(T_p - 273)^3 + 2.6572 \times 10^{-5}(T_p - 273)^2 - 4.8613 \times 10^{-5}(T_p - 273) + 8.342 \times 10^{-3}$$

The particle temperature is considered as the average surface temperature by assuming the particle Biot number < 0.1 considering it to be lumped mass. Relative activation energy correlation for 20% skim milk concentration is as follows [43],

$$\frac{\Delta E_v}{\Delta E_{v,b}} = -6.47438 \times 10^{-3}(X - X_b)^5 + 8.86858 \times 10^{-2}(X - X_b)^4 - 0.471097 \times (X - X_b)^3 + 1.22317(X - X_b)^2 - 1.62539(X - X_b) + 1.0092$$

Where $\Delta E_{v,b}$ is the equilibrium activation energy, X is the moisture content in the particle and X_b is the equilibrium moisture content. $\Delta E_{v,b}$ is calculated by the following equation

$$\Delta E_{v,b} = -RT_b ln\left(\frac{\rho_{v,b}}{\rho_{sat,b}}\right)$$

Where $\rho_{sat,b}$ is the saturation concentration based on gas temperature and $\rho_{v,b}$ is the bulk vapor concentration. X is calculated based on the mass fraction of water,

$$X = \frac{\omega_w}{1 - \omega_w}$$

Where ω_w is the mass fraction of water which is calculated by the following formula,

$$\omega_w = \phi_w \frac{M_w}{\phi_w M_w + \phi_m M_m}$$

Where ϕ_w is the mole fraction of water, ϕ_m is the mole fraction of milk solids, M_m is the molecular weight of milk solids and M_w is the molecular weight of milk solids. X_b is calculated from Guggenheim-Anderson-deBoer (GAB) model with parameters fitted for 20% solids skim milk.

$$X_b = \frac{m_0 C K a_w}{(1 - K a_w)(1 - K a_w + C K a_w)}$$

$$C = C_0 e^{\frac{\Delta H_1}{RT_b}} \quad K = K_0 e^{\frac{\Delta H_2}{RT_b}}$$

Where m_0 = 0.06156 kg/kg, C_0 = 0.001645, K_0 = 5.71, ΔH_1 = 24831 J/mol , ΔH_2 = -5118 J/mol , a_w is the water activity and T_b is the bulk gas temperature. a_w is calculated by Raoults law which

approximately corresponds to the mole fraction of water in the particle mixture.The temperature dependent $D_{air-vapor}$ is calculated by the following correlation [67],

$$D_{air-vapor} = 1.963 \times 10^{-7} T - 3.33307 \times 10^{-5}$$

Where, T is the gas temperature. The experimental case of single droplet drying reported by Lin et al. [68] is used as the base case to validate the REA model. In the experimental case, a milk droplet suspended using a glass filament is dried using the air flow. A 3-Dimensional transient multiphase simulation is performed numerically. In our case, gravitational and body force are neglected and the drag force is modified by returning the drag co-efficient to zero, so that the particle remains at a constant position which corresponds to a suspended droplet. The UDF codes for REA model can be found in the appendix D.

3.1.6 Numerical strategy

The numerical strategy is followed as reported in the literature [69, 70]. The momentum, energy, turbulence and species equations were spatially discretized using a second-order upwind scheme. Pressure equation was discretized using the PRESTO scheme, whereas pressure-velocity coupling was solved with SIMPLE scheme. Residuals and the outlet temperature were monitored during the numerical iterations. Convergence criteria were based on the residuals (10^{-4}). Discrete Phase Model (DPM) is introduced into the domain only after the continuous phase reaches a steady state. This ensured that discrete phase is solved in a stable manner. In milk drying case, multicomponent model is used to model milk by considering the solids as non-evaporating liquid particles, whereas droplet model is used to model spray drying of water.

3.1.7 Deposition model

When the particle temperature is above sticky point temperature while interacting with the wall boundary, it is assumed to stick. Although this an upper limit of deposition, this can be a simpler approach to account for deposition patterns realistically. In most literatures, the particle is simply removed from the domain and deposition rate is calculated. But it influences the temperature profiles and moisture content of gas, which in turn will affect the deposition. Therefore, it is assumed that all water in a particle is evaporated to the continuous phase, when the particle sticks. The sticky point temperature of skim milk is determined by adding 23.3 K to the glass transition temperature, as reported by Ozmen et al [71]. The glass transition temperature for skim milk is defined with Gordon Taylor equation as follows

$$Tg = \frac{\omega_1 T_{g1} + k\omega_2 T_{g2}}{\omega_1 + k\omega_2}$$

Where ω_1 is the mass fraction of milk solids, ω_2 is the mass fraction of water,T_{g1} is the glass transition temperature of amorphous lactose (101°C), T_{g2} is the glass transition temperature of water (-137°C) and k is the fitting constant of 7.4 for skim milk. The UDF codes for deposition model can be found in the appendix D.

3.1.8 Geometry and boundary conditions

The below geometry represents the fluid domain of the reactor, except for single droplet drying. The nozzle is located at the tip of the cylinder - 3 as shown in Fig.3 (Z=0). The feed is sprayed from top and hot air enters from the bottom. This fluid body is meshed in ANSYS Meshing with tetrahedral mesh and a mesh size of 3.5mm is found to be independent of mesh refinement through a mesh independence study (attached in appendix). The density and specific heat of skim milk are 1039 kg/m^3 and 3.97 kJ/kg-K respectively [47, 72]. For faster solution with lesser computational expense, tetrahedral cells are converted into polyhedral cells in ANSYS Fluent.

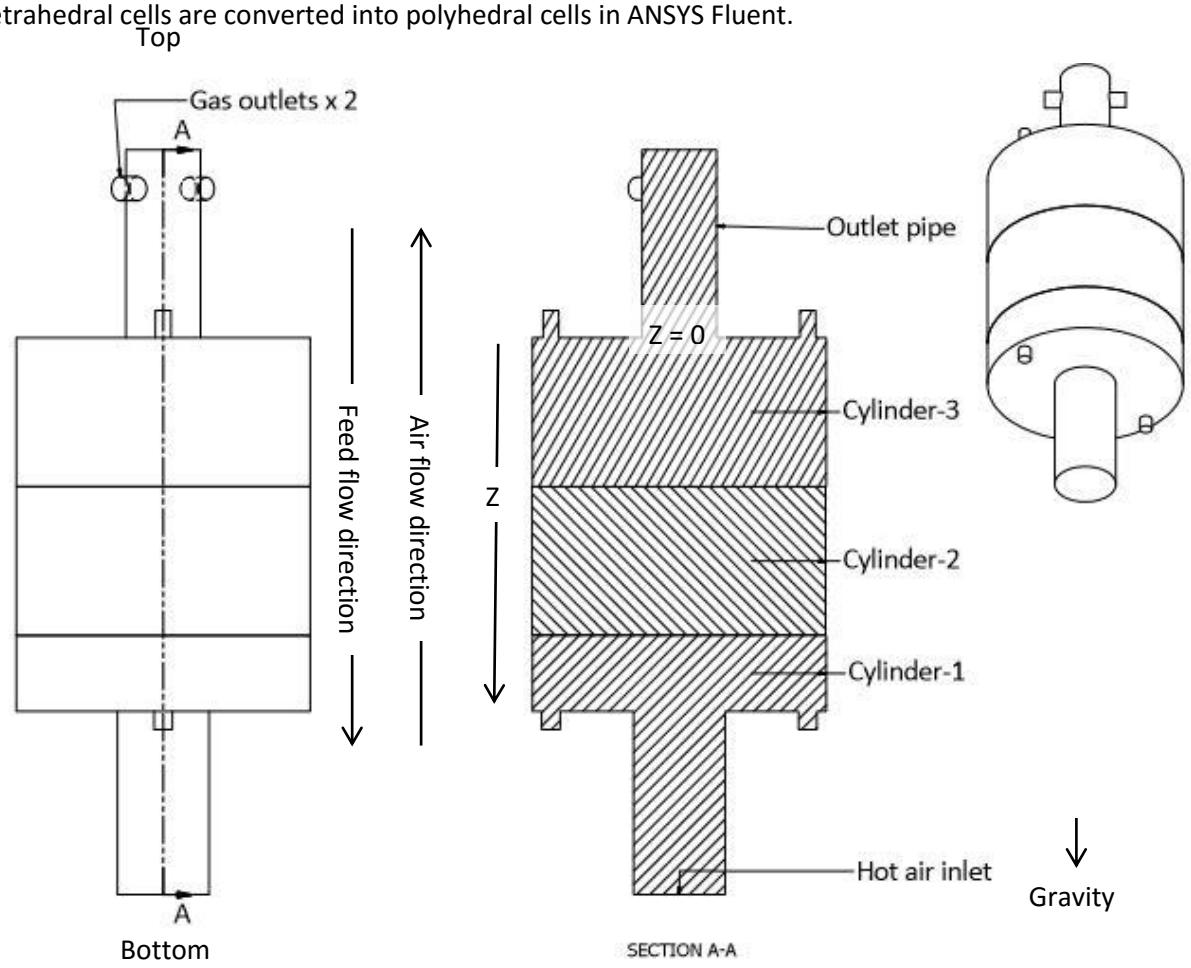

Fig.3 Reactor geometry

The injection velocities are calculated using the pressure drop based on Bernoulli's equation for 0.5 mm orifice diameter nozzle. The injection pressure for known feed flow rates are calculated using the nozzle calibration equations, they can be found in appendix. For a feed flow rate of 21.5 kg/hr , the injection pressure is estimated to be 49.4 bar. The heat transfer co-efficient is fitted to the experimental results as reported in the literature for effective modeling of heat transfer along the walls[35, 62]. The experimental diameter distribution data and their extrapolation can be found in appendix. The following tables show the boundary conditions for the reactor.

Continuous Phase	
Air inlet temperature	250°C
Air inlet - mass flow rate	480 (kg/hr)
Outlet pressure	Atmospheric pressure
Wall boundary condition	Convective heat transfer
Ambient temperature	25°C
Heat transfer co-efficient	$23W/m^2K$
Wall Material	Steel
Cylinder Wall thickness	3mm
Top and bottom plate thickness	10mm

Table.1 Continuous phase boundary conditions

Discrete Phase		
Injection type	Hollow cone - pressure nozzle	
Feed Flow rate	21.5 kg/hr	
Injection temperature	25°C	
Velocity(m/s)	98.47 m/s	
Actual nozzle position	Z= 0 cm	
Injection point	Z= 2 cm	
Half cone angle	14°	
Outer radius	5.49mm	
DPM boundary - gas outlets	Escape	
DPM boundary - Walls and Inlet	Reflect	
Feed type	Water	Milk
SMD(µm)	49.8	50.3
D90(µm)	95.19	97.5
D10(µm)	27.38	27.5

Table.2 Discrete phase boundary conditions

Injection type	Single
Injection temperature	23°C
Air inlet temperature	106.5°C
Air velocity	0.45 m/s
Time step	2.5×10^{-3} s
Particle diameter	1.44×10^{-3} m
Feed flow rate	2.338kg/hr
Injection start time	0 s
Injection stop time	2.5×10^{-3} s

Table.3 Boundary conditions - single droplet drying

3.2 Experimental Methodology

The model was experimentally validated on a counter-current lab-scale spray dryer fitted with a hollow cone pressure nozzle with orifice diameter of 0.5mm. The nozzle is fixed at Z = 0. The components of the setup are air control valve, heater, pump, frequency regulator, feed tank and cyclone. The volume flow rate of pressurized air is controlled by the control valve and heated to the required inlet temperature by using the heater. The feed rate is controlled by the frequency regulator. National Instruments C-series data acquisition modules are used. Labview 2017 is used to collect the data from the various sensors and control the process parameters through the above components. Two feed tanks are used to store milk and water; they are manually switched during experiments. Thermocouples (K-type) are used to determine gas temperatures. Five thermocouples are mounted radially and one 10 points thermocouple is mounted axially. Cyclone is used to separate the fine particles before the gas is allowed through exhaust. The dimensions of the drying chamber are as follows

Length of Air inlet	250.0 mm
Diameter of Air inlet	129.0 mm
Length of Cylinder-1	100.0 mm
Length of Cylinder-2	200.0 mm
Length of Cylinder-3	200.0 mm
Diameter of Cylinders	406.4 mm
Length of outlet pipe	250.0 mm
Diameter of outlet pipe	101.6 mm
Diameter of Gas outlet	38.0 mm

Table.4 drying chamber dimensions

The experimental study has been conducted in three stages. Initially hot air is introduced to flow through the chamber and heated gradually reaching the required temperature. It is allowed to heat up the reactor for some time. Then, water spray is introduced into the chamber and the process parameters for milk experiment are tested as it consumes lot of time in cleaning the reactor after each milk experiment. The optimum process conditions are chosen based on water experiments and they are used in the milk experiment. The reactor used in the experimental study can be found in Fig.4.

Fig.4 Experimental setup

4. RESULTS AND DISCUSSION

4.1 Experimental results

Two set of experiments were done with the above reactor. In the first experiment, drying of water spray was performed and reasonable conditions for drying were chosen. In the second experiment, spray drying of both water and milk were performed with the chosen process conditions. The relevant results for consistent process conditions are presented here and used as validation case of CFD models. The CFD boundary conditions are same as that of the process parameters used in the experiment

4.1.1 Experiment - Air only:

The below graphs (Fig.5,6) represent the initial heating period of the reactor

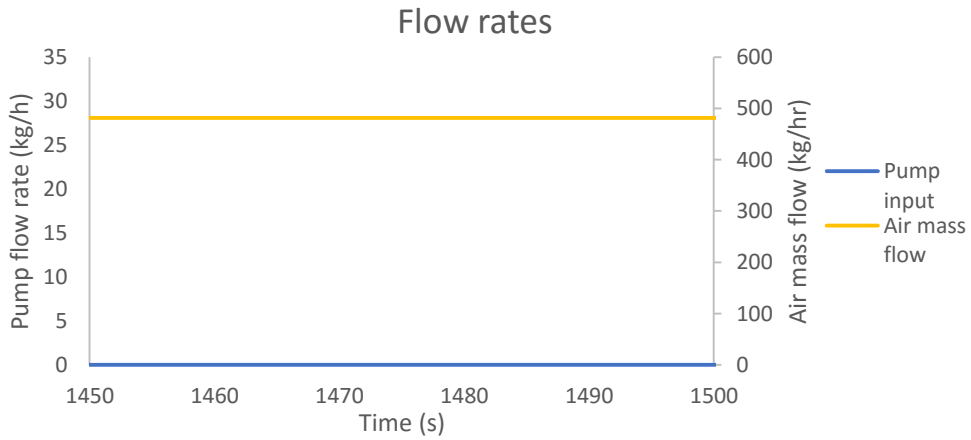

Fig.5 Flow rates

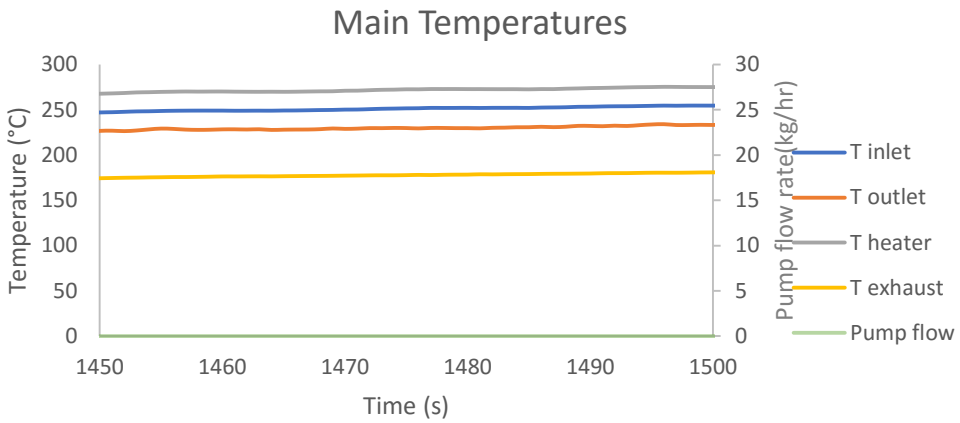

Fig.6 Main temperatures

From the main temperatures graph (Fig.7), it is found that there is an average temperature drop of 20°C between the inlet and outlet. So, it is essential to model for heat losses for better prediction of the drying process.

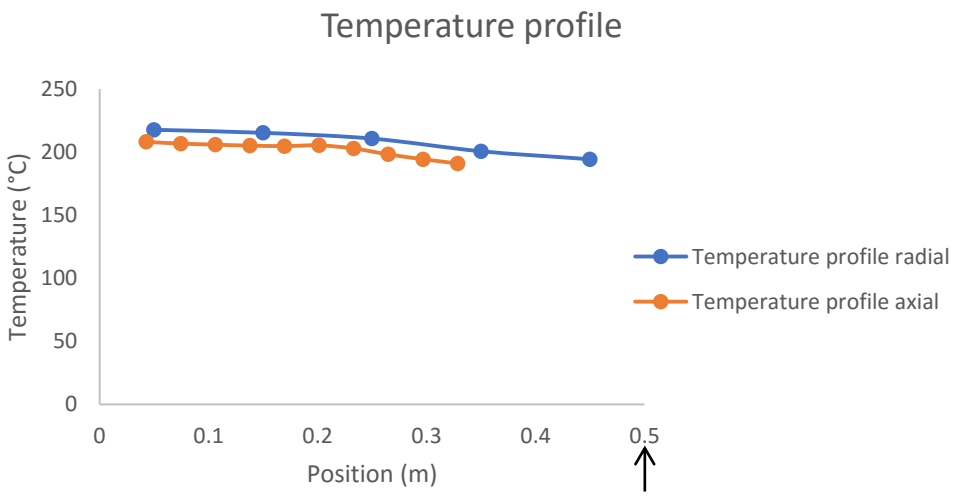

Fig.7 Temperature profile

Fig.7 represents the temperature profile inside the reactor at axial and radial thermocouple positions which are placed in two sides of the symmetrical axis. Although temperature trend is similar in both sides, it can be noted that the difference between radial and axial profiles shows that the flow is not perfectly symmetric for the reactor geometry. It can also be found that the temperature increases at thermocouple positions as the gas flows through the chamber. This could be because, the air flows in the center of the reactor, whereas thermocouples are positioned near the wall. This is also investigated in the CFD model.

4.1.2 Experiment - water

Water is often used as a pointer of milk in experimental research owing to its simple non-sticky nature and less complexity of physics involved compared to the milk drying. The feed flow is turned on, after the reactor is sufficiently heated up. The process conditions (see Fig.8,9) were maintained constant for a period of time so that the reactor reaches a steady state, to extract proper data for the process conditions. From the main temperature (Fig.9), it is observed that there is a temperature drop of 130°C, when water is sprayed into the reactor compared to the air only case. The temperature difference between air inlet and outlet is 150°C. This is a combined effect of water evaporation and heat losses.

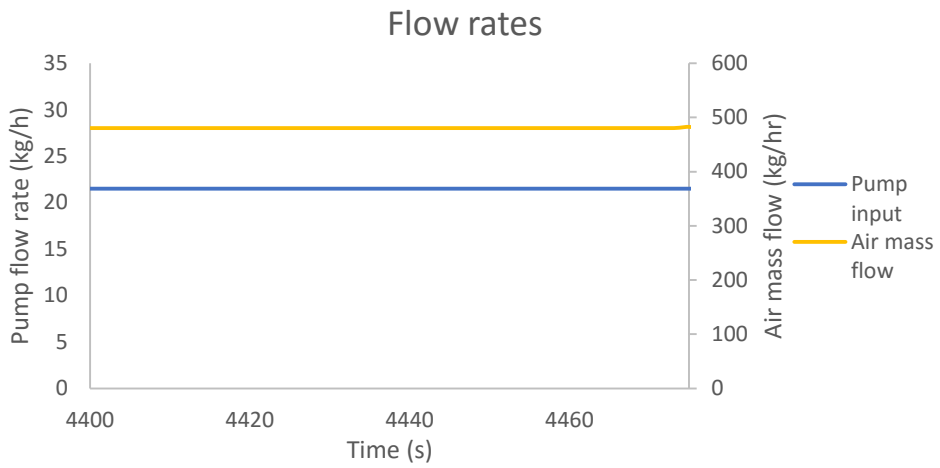

Fig.8 Flow rates

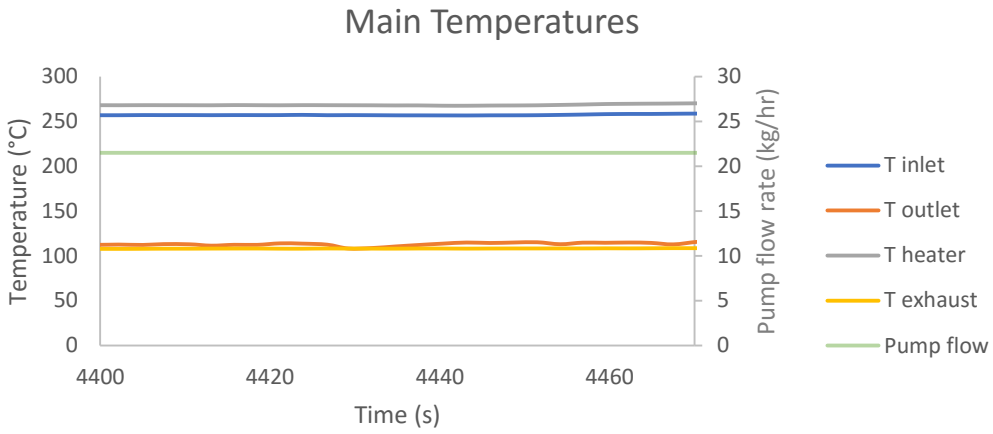

Fig.9 Main temperatures

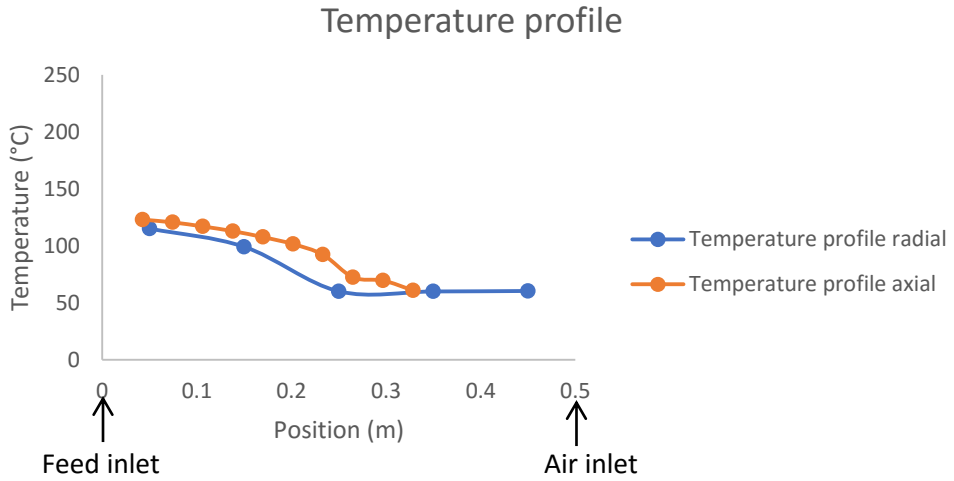

Fig.10 Temperature profile

From the Fig.10, it can be noted that the temperature drops an average of about 100°C till 0.2 m from the nozzle position, then there is a sudden increase in the temperature drop and remains almost constant till near air inlet region. This behavior could be due to the water impingement on the thermocouples, therefore they are further investigated in the CFD model.

4.1.3 Experiment - milk

This experiment is followed by that of water by change of feed to 20% skim milk, keeping all the process conditions same (Fig.11, 12). This ensured a one to one comparison of water and milk experiments, moreover direct introduction of milk at very high temperatures might lead to undesirable effects. From the following main temperature graph (Fig.12), it is observed that there is a temperature difference of 100°C between inlet and outlet temperatures, when water is sprayed into the reactor. When compared to the outlet temperature in water experiment, the outlet temperature is 50°C higher in milk experiment. This is because of the reduced water content, which corresponds to less consumption of heat for evaporation.

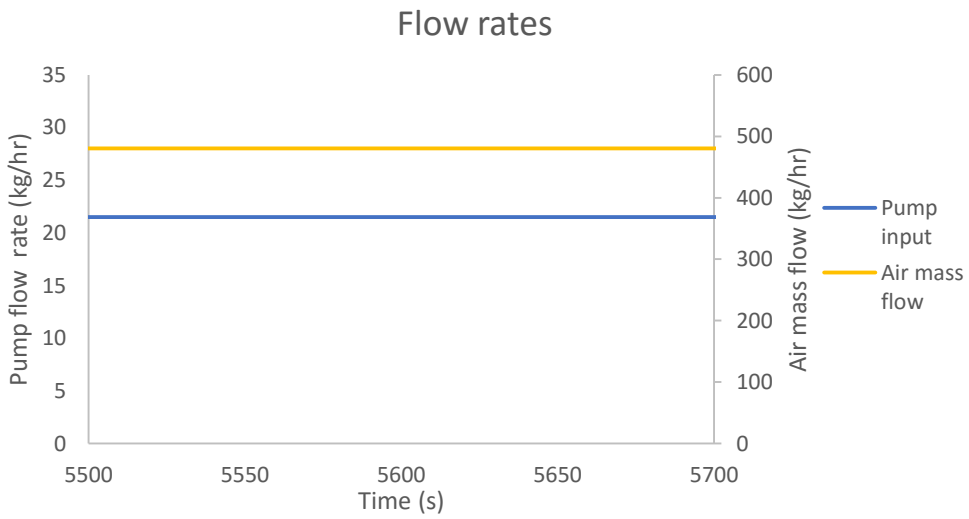

Fig.11 Flow rates

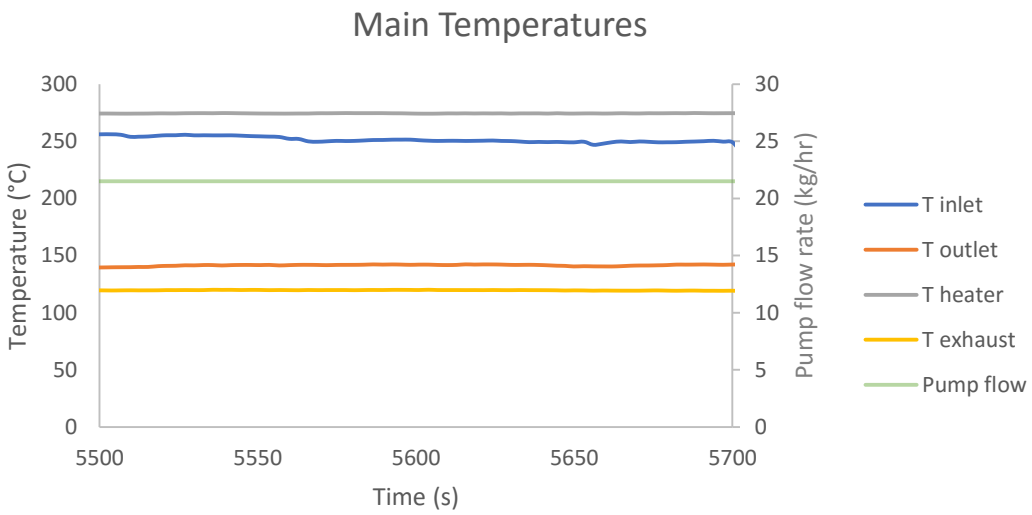

Fig.12 Main temperatures

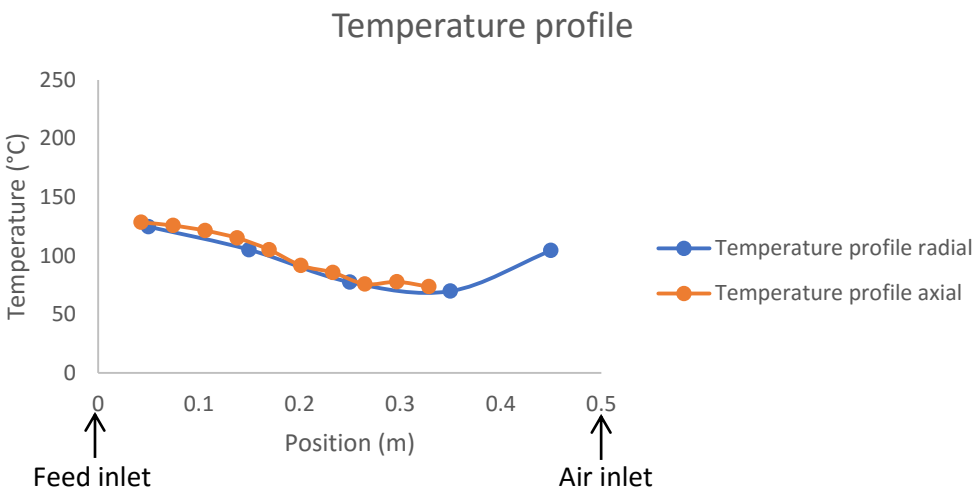

Fig.13 Temperature profile

From the temperature profile graph (Fig.13), it can be noted that the temperature profile has similar trend as that of water experiment, however the temperature inside the reactor has risen up by 10°C than that of water experiment, which corresponds to less water evaporation. It is found that the temperature near air inlet region shows a sudden jump from the decreasing trend. This difference in behavior compared to water could be because lesser water needs to be evaporated and therefore particles could have formed before reaching Z=0.45. It can also be observed that the axial and radial thermocouples show more symmetry in the flow with milk as the feed. In this experiment, considerable amount of milk deposition was found along the wall.

Reactor inside Fig.14

Cyclone inside Fig.15

Pump inlet- side plate Fig.16

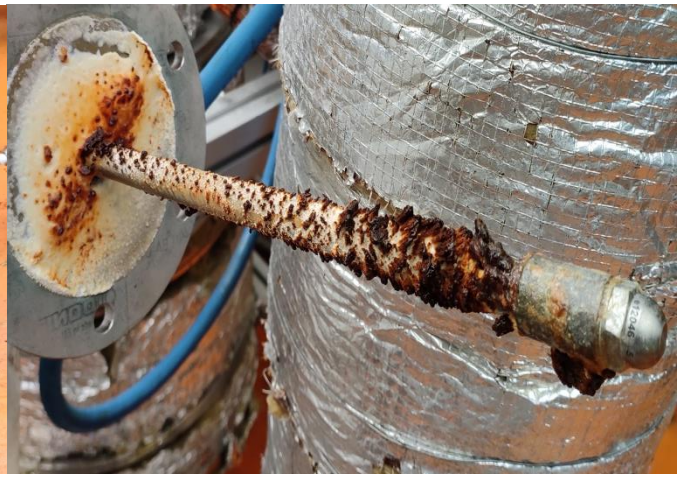

Nozzle pipe Fig.17

The above figures show that there is a considerable amount of milk deposited inside the reactor and further undergoes browning as it is exposed to hot air for a longer time. Furthermore, a good amount of whitish milk powder can be found in the cyclone (see Fig.15). It has been found that there is relatively no sticking in the cylinder-1 and the behavior is exhibited more as it moves closer to the near nozzle plate. Unexpectedly, the deposition trend is different in the air inlet side plate (see Fig.14), with semi-solid structures and dripping traces near the cylinder-1. The deposition behavior is further discussed qualitatively in comparison with the CFD deposition model.

4.2 CFD results

The CFD model is developed and validated in 5 parts: hot air only, water spray drying, single droplet drying, milk spray drying and wall deposition.

4.2.1 Single droplet drying

A fluid body of a simple cuboid with dimension 0.1 x 0.4 x 0.4 (m) is used for single droplet drying and meshed in ANSYS Meshing as the above case. It only has two boundary conditions, velocity inlet and a pressure outlet. Single droplet of 20% milk solids is introduced in the cuboidal domain using the multicomponent DPM model by introducing all the mass in a single time step. Initially, the default

drying model based on Raoult's law is compared with the experimental data. It is observed that evaporation happens linearly, in a much faster rate compared to the experimental data and evaporation stops with mass fraction of water reaching zero. But in the realistic case, the evaporation rate decreases with decrease in moisture content and particle moisture content never reaches zero. When REA is incorporated with default gas laws, the drying rate decreased and followed a similar trend with a significant difference in the drying rate. This is improved by incorporating the temperature based correlations for Air-vapor diffusivity. Thereafter, it is found that the numerical results nearly matches with experimental data, under predicted in the range of 50 to 100s and over predicted in the range of 200 to 250s. But overall it gives very close results to that of the experiments. Therefore it is concluded that the REA is implemented properly and it closely matches the realistic drying rates.

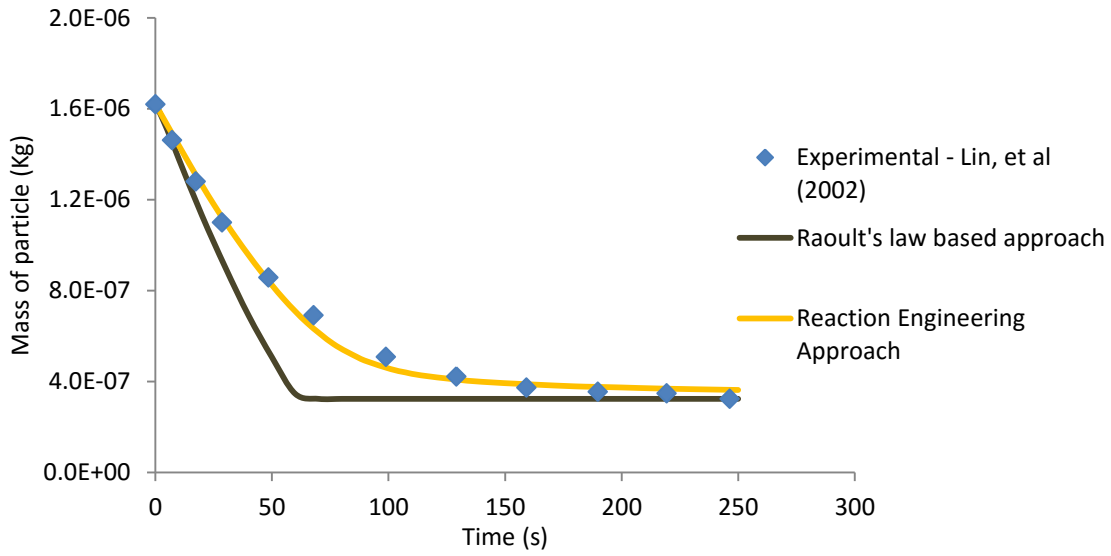

Fig.18 Single droplet validation

4.2.2 Heat loss model

The initial heating period of the reactor is used as the base for modeling heat losses with reference to outlet temperature of 230°C. The process conditions used for heating up the reactor only has the hot air flow in the reactor without spray. The heat losses through wall are modeled by adding a thin wall along with thermal wall boundary conditions. The thermal resistance $\left(\frac{\Delta x}{k}\right)$ is used to solve for conduction based on thin wall of specified thickness (Δx) and thermal conductivity of material(k). The corresponding exterior wall temperature is used to calculate the heat transfer based on convective heat transfer co-efficient and free stream temperature. The thermocouple readings inside the reactor are compared against the predicted temperatures at the same positions to validate for heat losses.

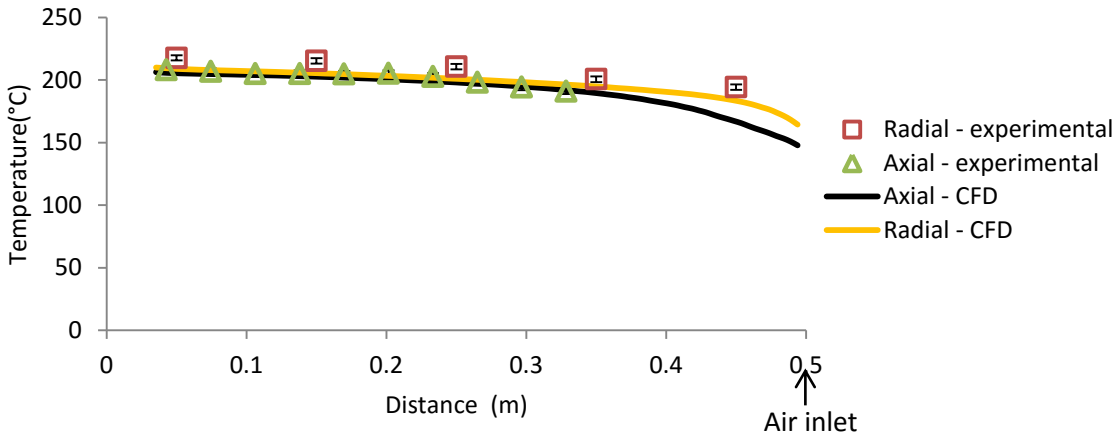

Fig.19 Temperature profiles - CFD vs Experimental comparison

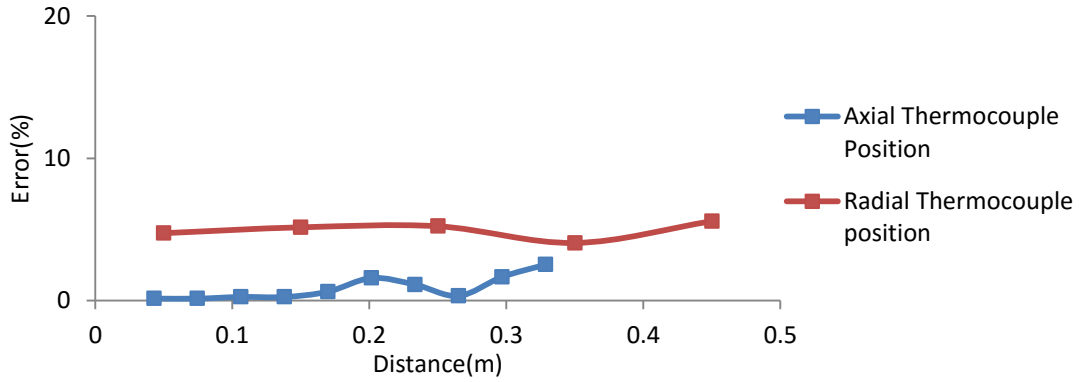

Fig.20 Error graph - CFD vs Experimental comparison

The above comparison of temperature at different heights (Fig.19) indicates a match of the heat loss during experiments with the numerical results. For precise difference in the data, the relative error is computed. The error graph (Fig.20) shows that axial profiles are very close the experimental results, whereas radial profile on an average has 5% error. It can also be understood both from experimental and CFD profiles that the flow is not absolutely symmetric as it nears the air inlet region which has more dead zones and recirculation zones. From the temperature contour (Fig.21), it is observable that the flow does not expand instantly, the thermal boundary layer develops as it flows through the chamber, which is due to thermal dissipation outwards the core flow and a part of hot air flow which is bounced back at the bottom plate, causing a recirculation at nozzle side. Furthermore, the radial regions adjacent to the air inlet remain cold as dead zones showing low temperatures along the top plate. But then the upper part of the reactor remains relatively a dead zone with lower temperature and lower air flow.

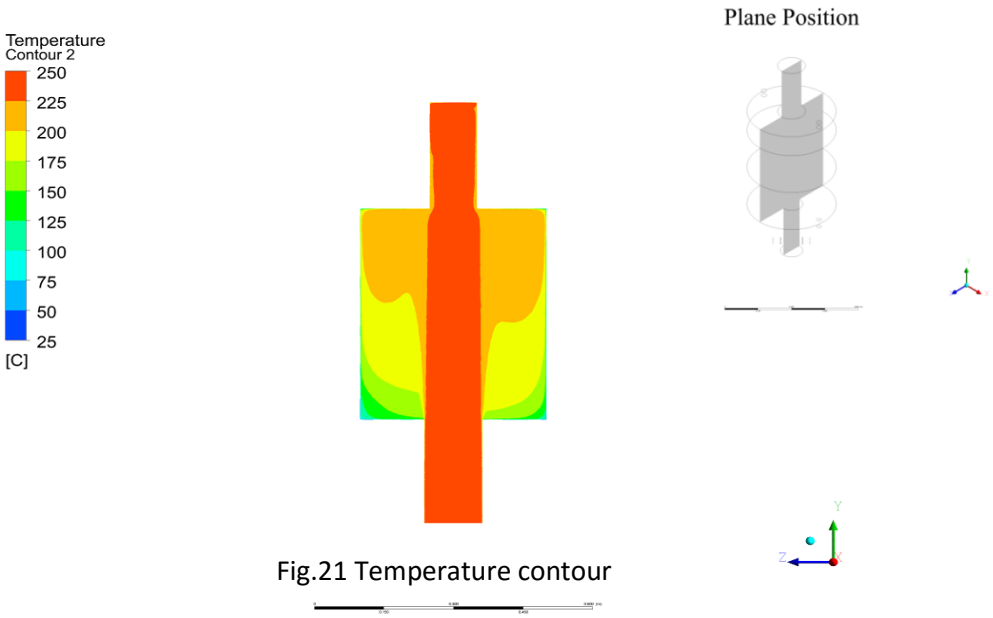

Fig.21 Temperature contour

4.2.3 Water drying model

It is essential to model evaporation of water droplets as it is often used before drying milk in experimental cases. The water droplet case is computationally solved and the results are evaluated at the thermocouple positions. It can be seen from the Fig.22, that there is a close similarity with first few positions and gets closer at near the air inlet, but there is a deviation in the mid profiles. This can be due to wetting of thermocouples which was observed during the experiments. When compared with air only graph, the trend remains same but just that temperature drops due to heat of evaporation. This temperature drop is mainly due to the latent heat absorbed by water droplets for evaporation.

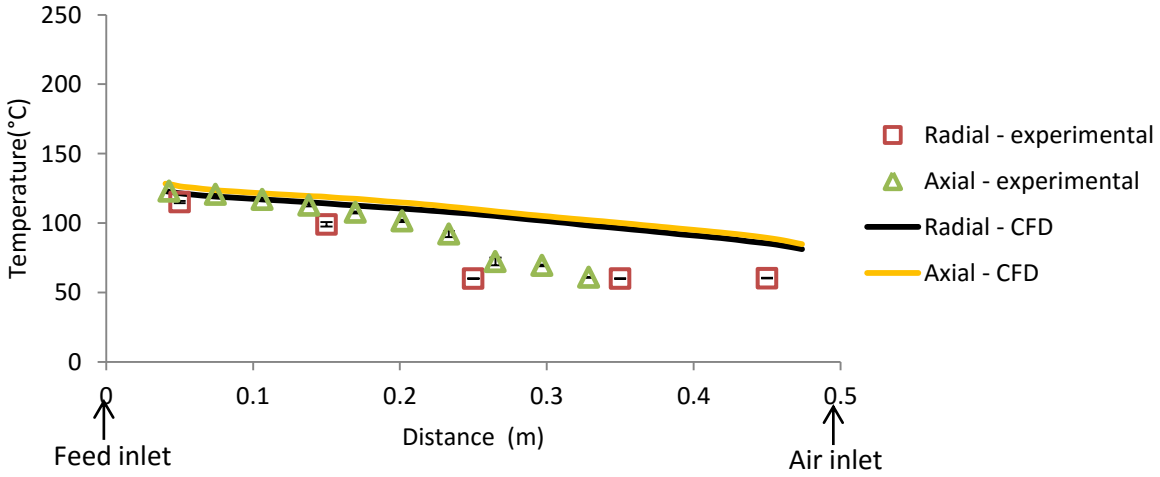

Fig.22 Temperature profiles - CFD vs Experimental comparison

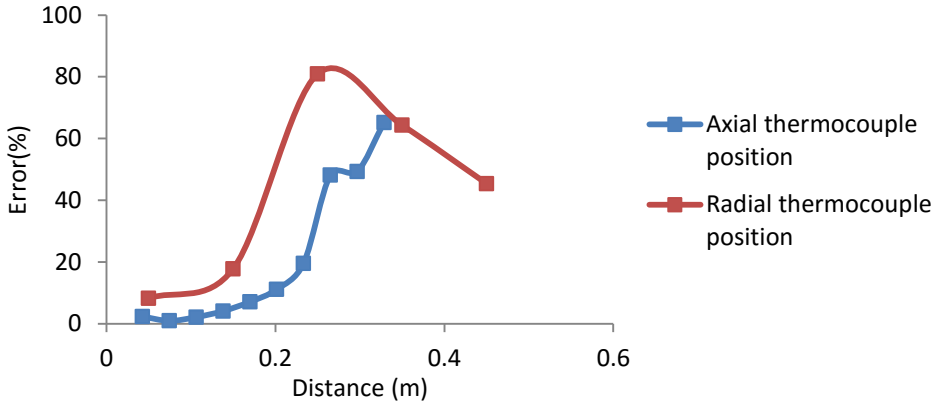

Fig.23 Error graph - CFD vs Experimental comparison

The CFD results matches well till Z=0.15m and average error increases as moved further away (see Fig.23), but decreases after a point at Z=0.25m (80% error), whereas the error at Z=0.45 is about 45%. The net average error was found to be 32%. Therefore, to understand this difference, the droplet trajectories are plotted as a function of water mass to show the droplet impingement at the thermocouple positions (Fig.24,25).

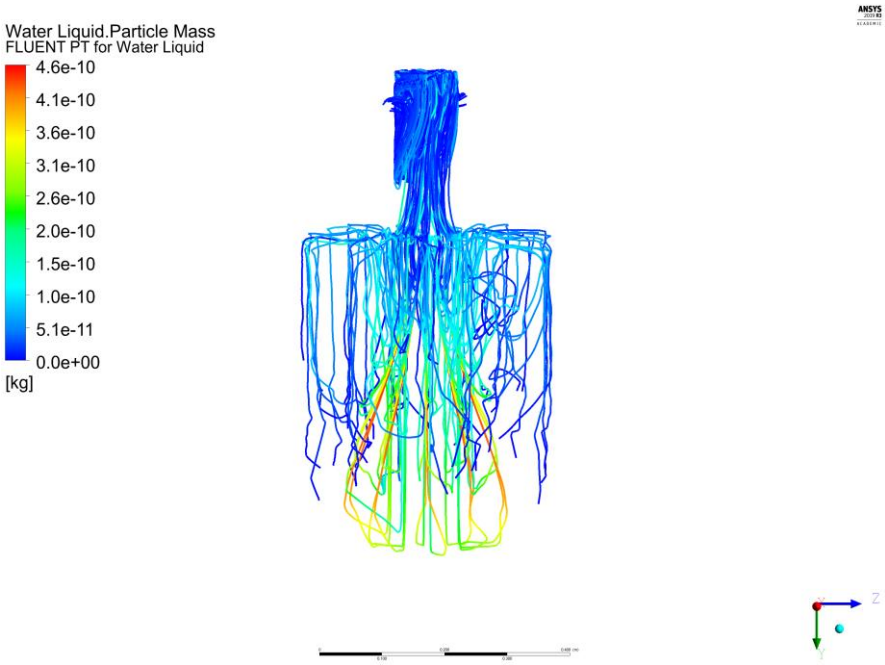

Fig.24 Particle trajectory as a function of mass

The Fig.24 explains the evaporation of water droplets and it can be observed that the non-evaporated water droplets strike directly towards the air inlet and the evaporation is more observed in the bottom part of the reactor and this can be compared with the temperature contour of air-only solution, where the temperature is higher at the bottom with lower temperatures of dead zones in the top. It is found that the bigger droplets move towards air inlet, whereas the smaller droplets are instantly deflected upwards and evaporated there. Furthermore to clarify the inflection point for error in the mid of the reactor, the thermocouple positions are evaluated (see Fig.25).

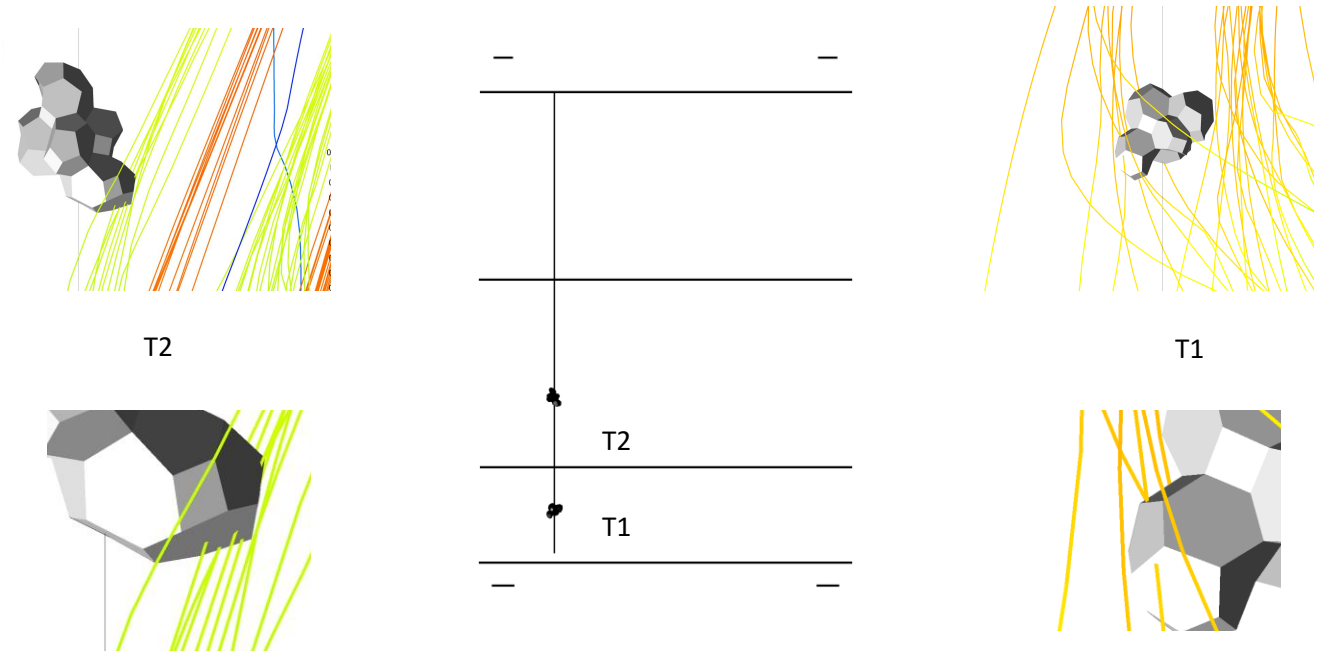

Fig.25 Thermocouple wetting

T1 represents the radial thermocouple position at Z=0.45 m and T2 represents the radial thermocouple position at Z=0.33 m. The error drops at T1, after attaining maximum error at T2 (see Fig.23). T2 is directly hit by the injected water droplets, whereas T1 is hit by the water droplets with a trajectory in the opposite direction to that of T2 (see Fig.25). This direction change is shown through the curved trajectory, which represents the droplet hitting along the wall. In real case, a part of water splashes and rest forms film on the wall. This explains the increasing and decreasing temperature trends with inflection point at the mid-section.

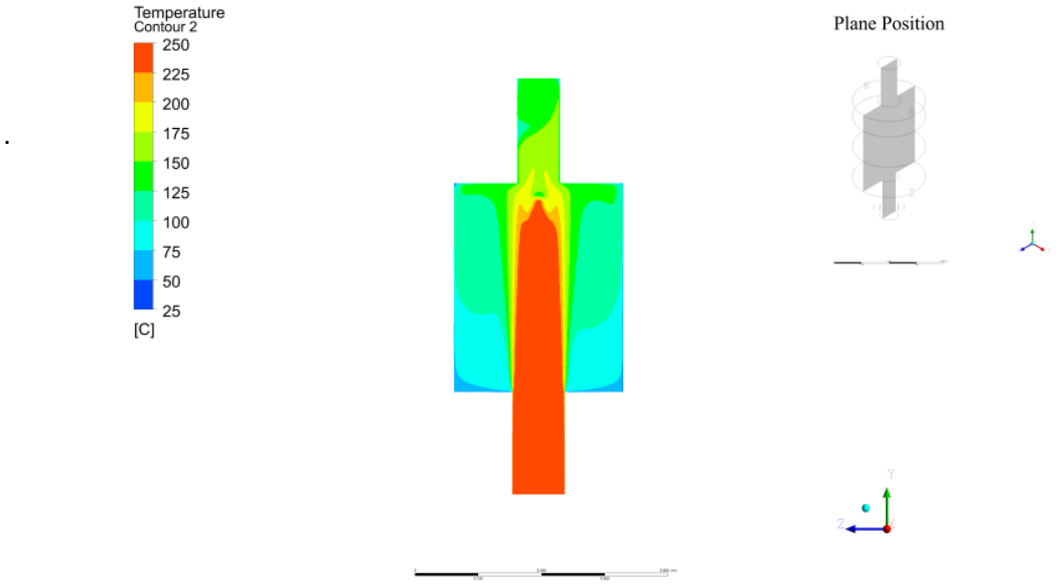

Fig.26 Temperature contour

Fig.26 and Fig.27 shows temperature contour and water mass fraction contour respectively. From the temperature contour, it is observable that the temperature drops as soon as it contacts with the spray. The core region of the hot air converges as it comes closer to the nozzle injection point in the hollow space of the conical spray. Comparing temperature contour and droplet trajectory (see Fig.24,26), it can observed that angle of droplets in the moving spray is widened by the counter-flowing air. Similarly, water mass fraction contour in comparison with temperature contour shows that the mass fraction of water vapor increases with decrease in temperature, which could be due to the absorption of latent heat by the water droplet which corresponds to increase in the water vapor fraction in the continuous phase. This increase in absolute humidity also influences the wet bulb temperature at these points adding to the effects of water impingement in decreased experimental temperatures.

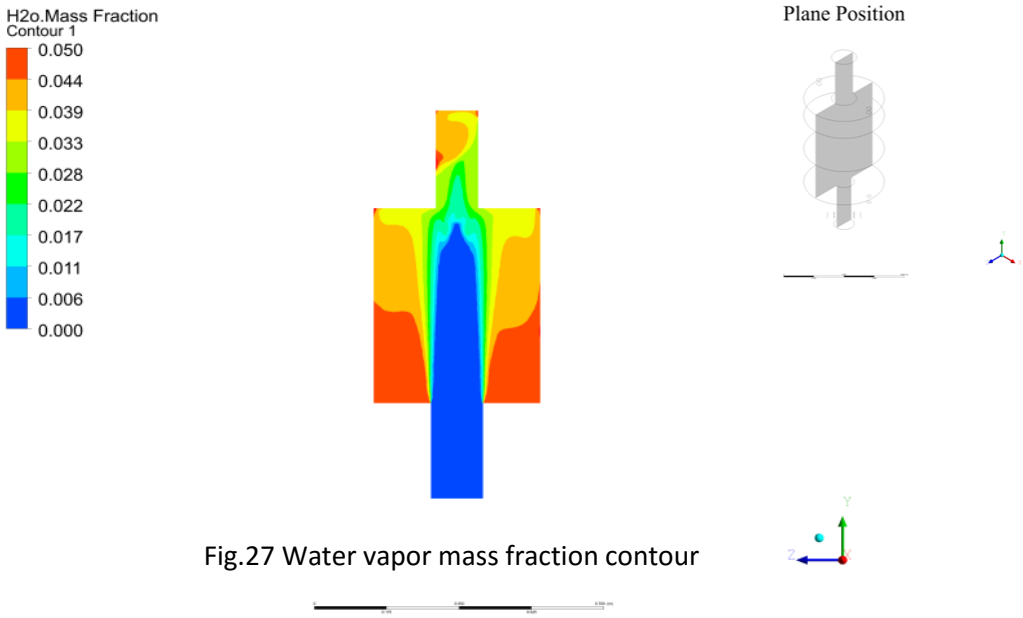

Fig.27 Water vapor mass fraction contour

4.2.4 Milk drying model

The validated REA model is implemented with the multicomponent model for modeling of skim milk droplets.

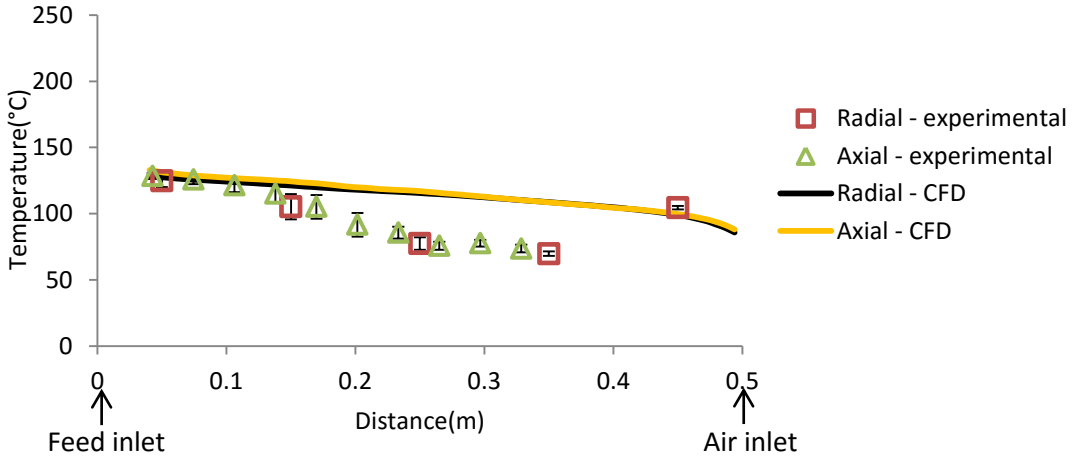

Fig.28 Temperature profile - CFD vs Experimental

Fig.28 shows the temperature profiles comparing experimental and CFD results. Fig.29 shows the relative error between experimental and CFD results. It is found that the CFD model predicts closely to that of experimental case till Z=0.1m (Fig.28), however the error (Fig.29) gradually increases and decreases after an inflection point at Z=0.35. This pattern is similar to that of water evaporation, but the interesting point is that the error almost goes very low such that error at Z=0.45m is around 4%, which is 45% for water experiment. The net average error was found to be 26% compared to 32% for water case.

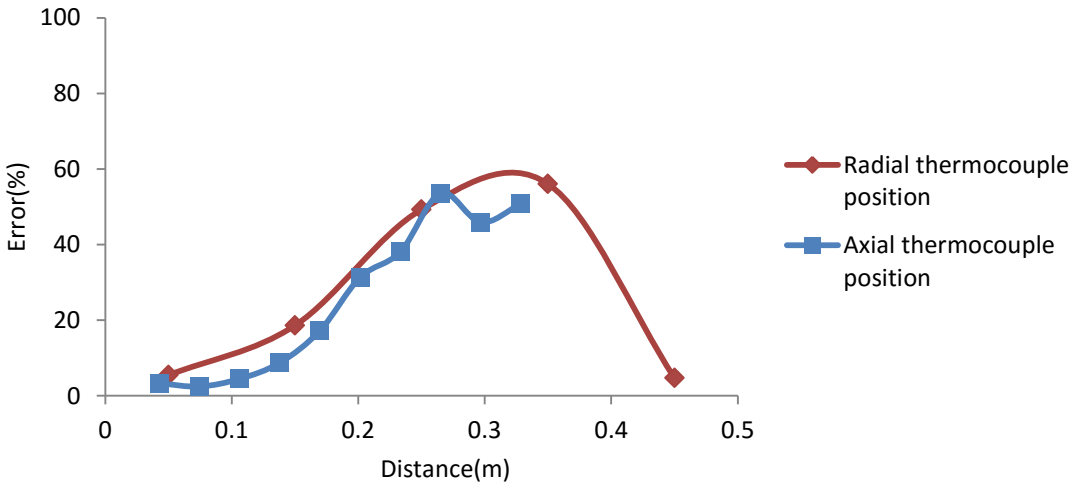

Fig.29 Error graph - CFD vs Experimental comparison

The difference in the error can be explained in terms of reduced water content and correspondingly lower wetting of thermocouple. Furthermore, the water vapor mass fraction contour (Fig.30) explains the difference in the net evaporation compared to the water case. It can be observed that the mass fraction in the regions around air inlet is around 0.04 for milk, whereas it is around 0.05 for water. The significant difference in error at Z=0.45m can be explained as an effect of increased density correspondingly the momentum, which leads to more widening of the spray at this region such that this thermocouple point is not as wetted as in the water case. This is explained by comparing T1 positions of water (Fig.25) and milk (Fig.31).

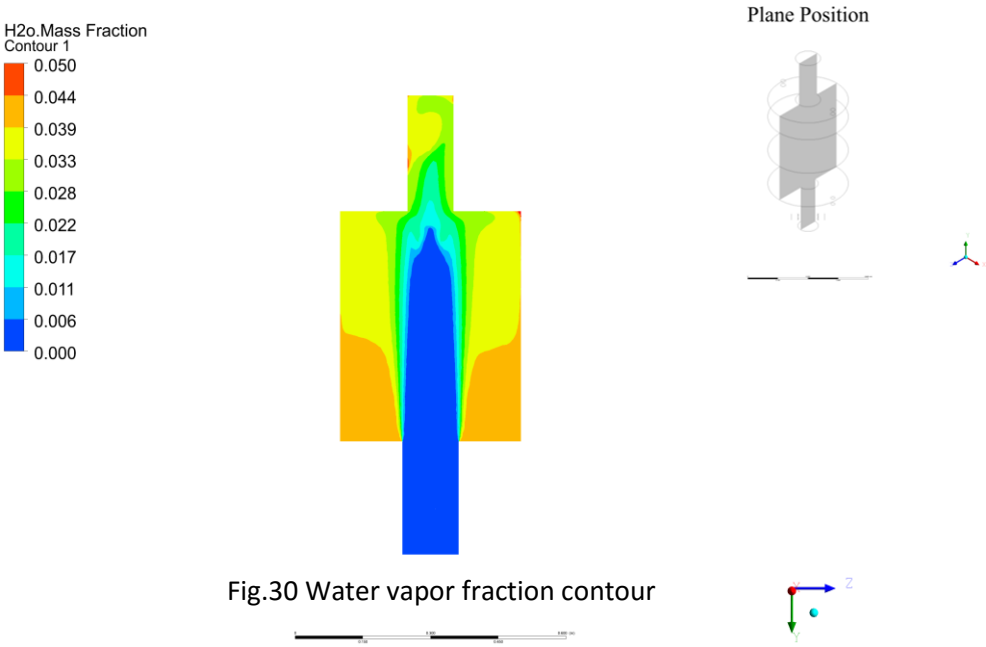

Fig.30 Water vapor fraction contour

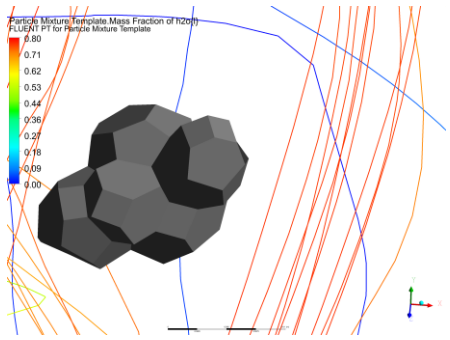

Fig.31 T1 - Milk

The temperature contour of milk (Fig.32) is compared with that of water case (Fig. 26). It can be observed that in the milk case temperature along top plate is higher water evaporation case. It is more evident that the near nozzle region has comparatively high temperatures. This could be an effect of lower water content and further influence of kinetic hindrance in the evaporation of multicomponent mixture compared to pure water.

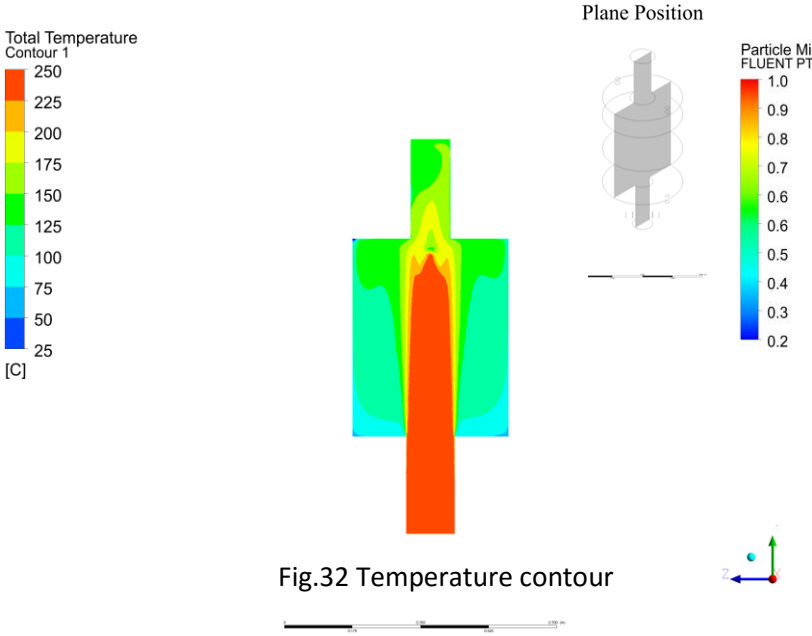

Fig.32 Temperature contour

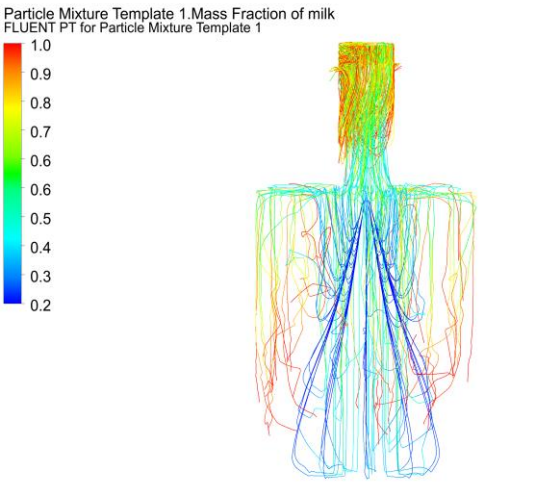

Fig.33 Particle trajectory as a function of milk solid mass fraction

The formation of dried powder can be understood through the particle trajectory of mass fraction of milk. Fig.33 shows that the mass fraction of milk is highly variable depending on the path that a particle takes. The particle path is highly influenced by its initial mass which corresponds to the initial diameter of the droplet. Therefore, the particles are categorized based on their particle diameter, so that it is easy to understand the behavior of dried powder formation.

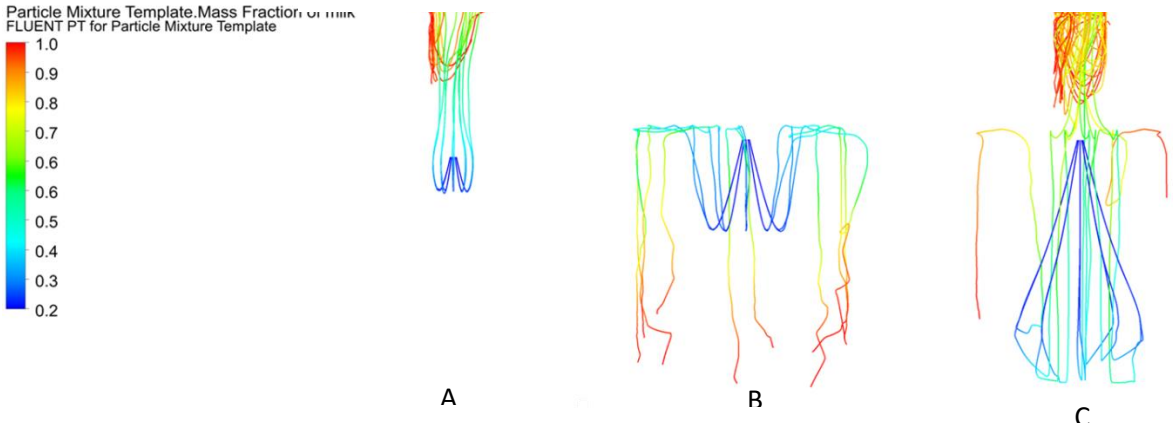

Fig.34 Particle trajectories as a function of milk solid mass fraction

A) Particle diameter < 55 µm B) 55 µm < Particle diameter < 85 µm C) Particle diameter > 85 µm

From the above particle trajectories, it is observable that almost all particles which have initial diameter less than 55 µm does not enter the chamber but directly moves to the outlet pipe and the higher mass fraction of milk is observed inside the outlet pipe where most of the evaporation takes place for these droplets. For the particles with initial diameter between 55 µm and 85 µm, the droplets further penetrate into the chamber as well as radial opening is seen. They hit back the plate near the nozzle, further moving down along the cylinder wall. This behavior is very close to that of gas obstructed by the nozzle side plate, therefore these particles travel along the movement of gas in the chamber. In this case, higher mass fraction of milk is found in the regions of cylinder -1 and cylinder-2. In case of particles with diameter above 85 µm, the droplets are not easily influenced by the gas, thereby penetrate further, get reflected from the inlet side plate and then get into the full influence of air stream. The milk particles are formed in the outlet pipe region. In all the above cases, it is found that the initial momentum of the droplets actually influence the trajectory, the droplets get into the influence of gas flow once their downward momentum reaches zero. To further understand the evaporation in different initial droplet sizes, the mass and temperature of particles with diameters chosen from three ranges are plotted as a function of time (Fig.36).

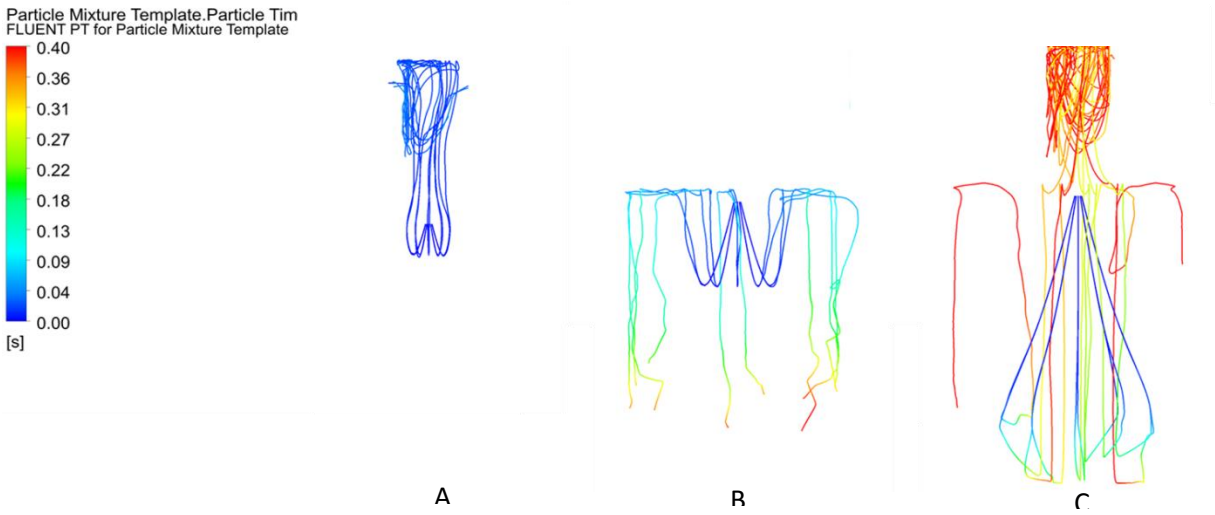

Fig.35 Particle trajectories as a function of time

A) Particle diameter < 55 µm B) 55 µm < Particle diameter < 85 µm C) Particle diameter > 85 µm

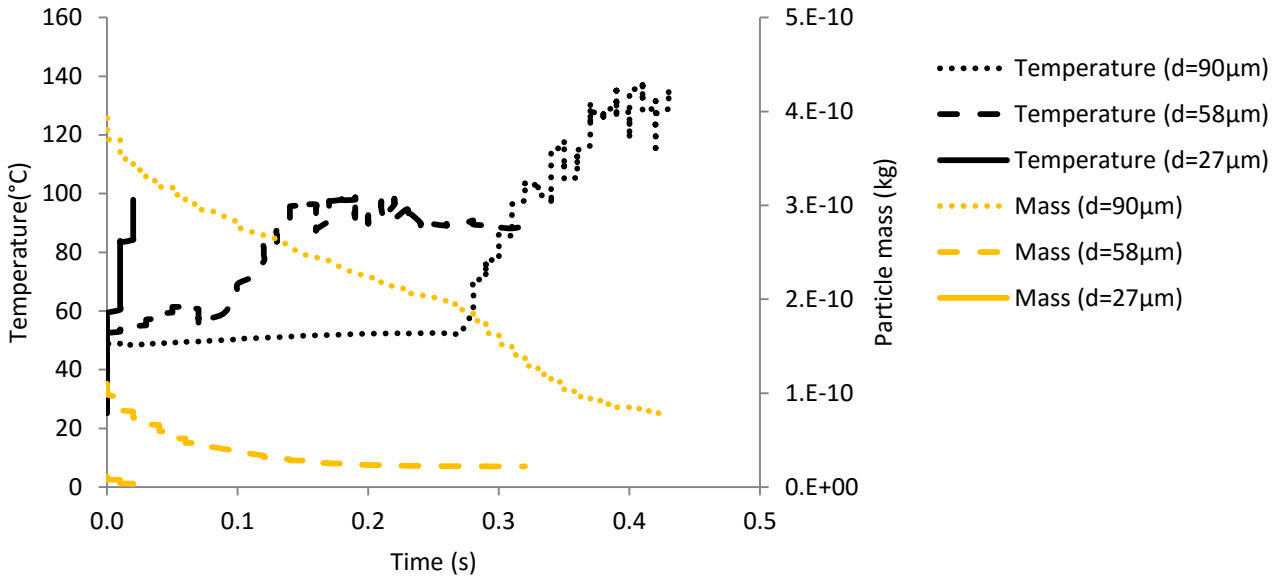

Fig.36 Particle Temperature and mass

For the particle with initial diameter of 27 µm, the residence time is too low (0.02s) as it flows into the outlet pipe almost instantaneously(see Fig.35), even then the temperature has risen up so fast and evaporated to form the milk powder (see Fig.34). In case of 58 µm particles, they have a considerable residence time (0.31s) flowing through the cylinder walls and evaporation happens so gradually very similar to a single droplet case. But the rate of increase in temperature shifts up at 0.07s when the flow direction is changed along the direction of air. The temperature and mass of the particle have very small water left after 0.15 s , therefore the temperature and mass of the particle remain nearly consistent. For the particle with initial diameter of 90 µm, the residence time is higher (0.42s), the temperature increases very slowly till 0.26s and the rate of increase is drastically shifted up. Similarly, the evaporation rate also increased at the same time. This change in rates is similar to the trends in all diameter ranges and this point of change is related to the change in flow direction along the gas flow. The temperature fluctuations are observed when the particle is in full influence of gas flow, this could be due to high fluctuation of particle movements in different regions.

4.2.5 Wall deposition model

The wall deposition model based on sticky point temperature has been implemented and the results are as follows

Wall	Deposition rate (kg/hr)
Nozzle side plate	2.420
Cylinder-3	0.210
Cylinder-2	0.000
Cylinder-1	0.000
Air side plate	0.003
Outlet pipe	1.620

Table.5 Deposition rates

It is found that nearly half of injected milk is deposited in the plate near the nozzle, followed by a significant deposition at the outlet pipe. The below table explains that majority of the injected milk is deposited over the walls. Only 1% goes out of the setup as free particles. It is also notable that there

is almost no deposition in the cylinders 1 and 2. In order to understand the realistic validity of this model, the deposition patterns are qualitatively compared as below

Net Deposition rate (kg/hr)	4.256
Net solids Injection rate (kg/hr)	4.300
Free Powder production rate(kg/hr)	0.044

Table.6 Mass balance

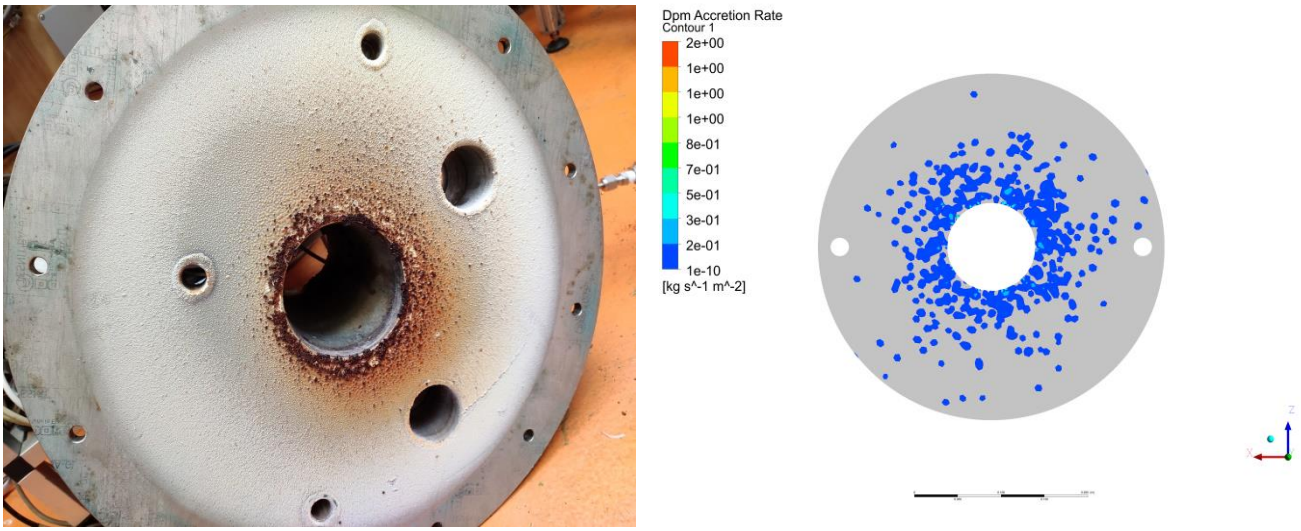

Fig.37 Nozzle side

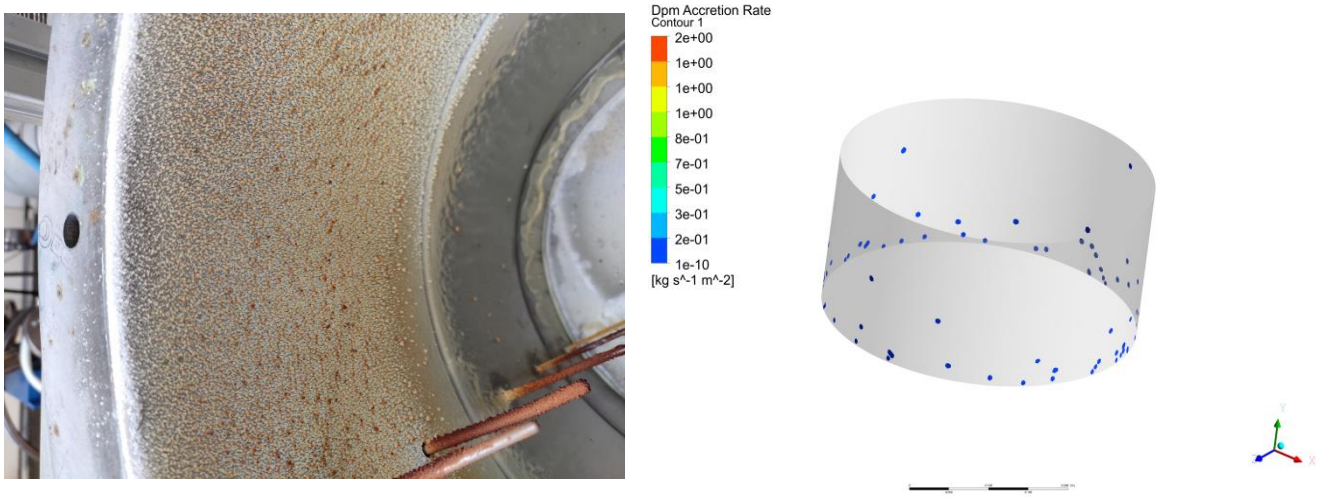

Fig.38 Cylinder - 3

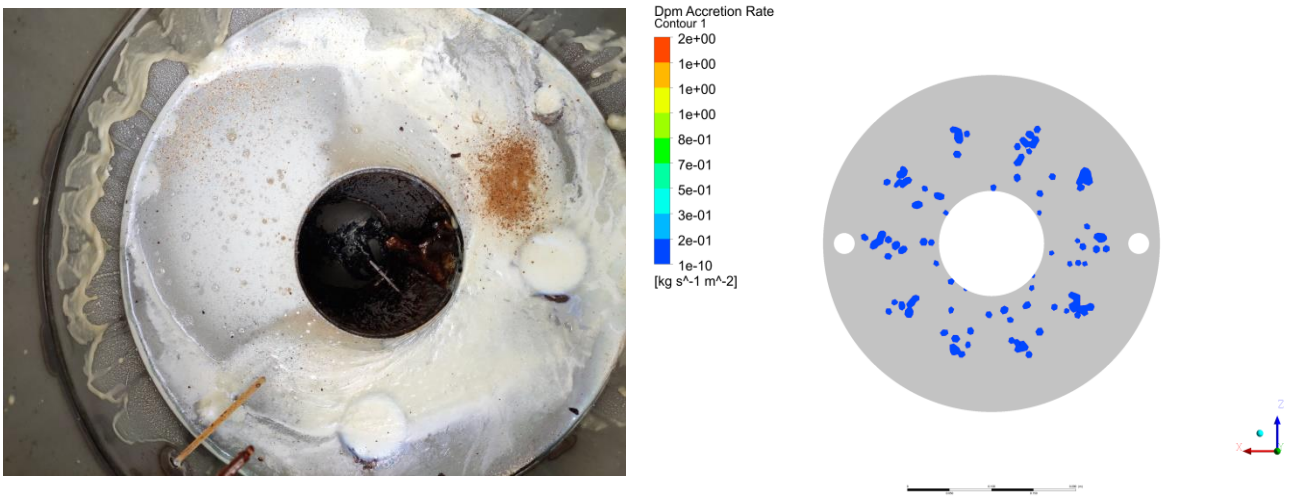

Fig.39 Air inlet side

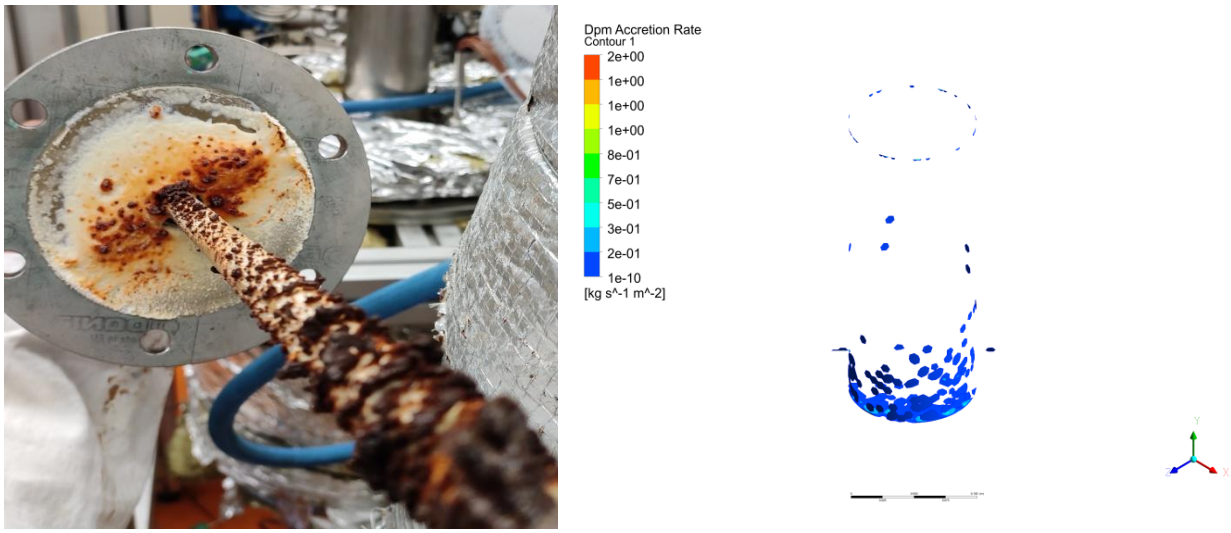

Fig.40 Outlet pipe

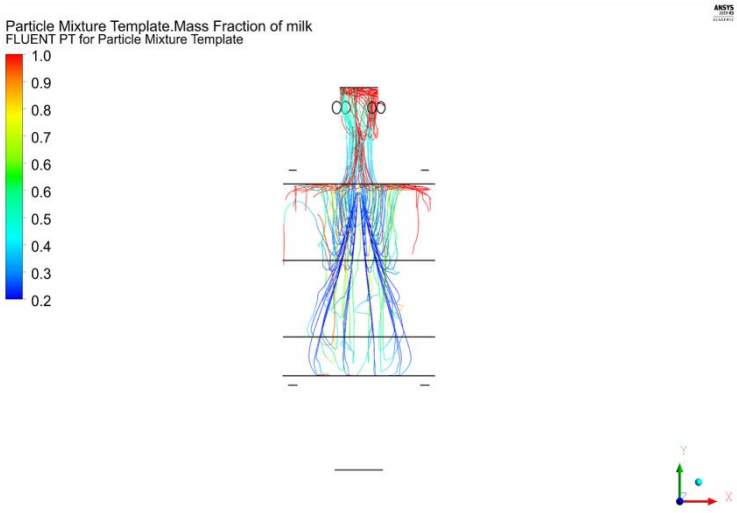

Fig.41 Trajectory of sticking particles as a function of milk solid mass fraction

From the experimental picture of cylinder – 3, it can be observed that there is almost no deposition beyond cylinder – 1 till cylinder - 3 as found in the CFD results. The above pictures show qualitatively, that the deposition patterns are quite similar for CFD results when compared with experimental results of other walls as well. In the nozzle side plate, outlet pipe flange and cylinder – 3, it is found that the particles have deposited in the wall and more browning is observed in these regions (experimental results). This behavior is mainly because the core flow region that hits these walls is relatively hotter than the other regions as found in the temperature contour of milk results (Fig.32). However, in the experimental results, the air inlet side plate has more semi-solid particles with patterns of wall films (Fig.39). This behavior is mainly due to low temperature in the dead zones near the air inlet side as observed in the temperature contour of milk model. It is also observable from trajectory of sticking particles, that most of them are undried milk. Therefore it is concluded that this model predicts the deposition patterns well, but not the deposition rates accurately as there are many free particles found in the cyclone experimental picture.

5. CONCLUSIONS AND RECOMMENDATIONS

In this study, three dimensional steady state CFD model is developed for counter flow spray dryer setup. A multiphase model using Eulerian - Lagrangian approach is employed along with two way coupling. The model is experimentally validated with air, water and skim milk experiments using temperature measurements at various heights. The heat loss model is developed and incorporated in the air only case. Further, the CFD results are compared to that of experimental results and 5% average error is found, thereby validating the heat loss model. REA drying model is developed based on single droplet experiments as reported in the literature and matching results were found. It has also been found that the particle diameter ranges are influential in determining the particle trajectory and their residence time. The smaller particles have higher evaporation rate. The particle temperature drastically increases after the change in momentum direction. The average errors of CFD results with respect to the experimental results are found to be 32% and 26% water and milk drying cases respectively. Therefore it is concluded that model shows good agreement with the experimental results. It is notable that the average error in milk with 80% water is lower than pure water. The major errors were found to be caused by water impingement and humidity influence over the thermocouples. A close similarity between milk and water cases is found with slight difference in the temperature profile trends. The trend difference is due to the density difference between the two feeds. The deposition model is developed based on the sticky point temperature and incorporated along with REA model. The model shows good qualitative agreement depicting most browned particles at nozzle plate and big particle deposition at air side plate which in experiments was observed as semi-solid milk accumulation. It has been found that 98% of injected mass stick to the reactor walls and only 2% of injected mass form as milk particles. The deposition is found to be high near the nozzle and reduces towards the air inlet. This pattern is comparable in both CFD and experimental results. Although quantitative study has not been done, the difference in the deposition rate is quantitatively observable as some whitish particles are found in the cyclone in experimental case, whereas in CFD most particles stick for this case. Because, this model solely depends on the sticky point temperature. In real cases, there are other factors like particle-wall, particle-particle collisions based on visco-elastic forces and surface tension of droplets. Therefore it is recommended that for more accurate quantitative modeling, the current model could be extended with the models incorporating wall films, wall temperature, surface tension and visco-elastic forces of the droplets. In case of experiments, it is recommended to extract more temperature and humidity data inside the chamber at different radial and axial positions. Furthermore, the study for wall deposition could be extended quantitatively by measuring the weight of milk deposits along the wall. This will be very helpful in effective modeling of wall deposition.

REFERENCES

1. Bahnasawy, A., A. Okasha, and E. Gonbeej, *Performance evaluation of a laboratory scale spray dryer.* Misr J Ag Eng, 2010. **27**(1): p. 326-46.
2. Vass, P., et al., *Drying technology strategies for colon-targeted oral delivery of biopharmaceuticals.* Journal of Controlled Release, 2019. **296**.
3. Tamime, A.Y., *Dairy powders and concentrated products*. 2009: John Wiley & Sons.
4. Engmann, F., *Spray Drying as an Appropriate Technology for the Food and Pharmaceutical Industries - A Review.* Journal of Environmental Science, Computer Science and Engineering & Technology, 2013. **1**: p. 467-476.
5. *Introduction to spray drying*, in *Spray Drying Techniques for Food Ingredient Encapsulation*. p. 1-36.
6. *Radial Multizone Dryer (RMZD) : https://www.utwente.nl/en/et/tfe/research-groups/TE/research/projects/Radial%20Multi-Zone%20Dryer/#project-information*.
7. Keey, R.B. and Q.T. Pham, *BEHAVIOUR OF SPRAY DRYERS WITH NOZZLE ATOMISERS.* Chemical Engineer (London), 1976(311): p. 516-521.
8. *Basics of Nozzle Technology*. Available from: https://www.lechler.com/de-en/technology/basics-nozzle-technology/atomization-methods/pneumatic-atomization/.
9. Bellinghausen, R., *Spray drying from yesterday to tomorrow: An industrial perspective.* Drying Technology, 2019. **37**(5): p. 612-622.
10. Patel, R., M. Patel, and A. Suthar, *Spray drying technology: an overview.* Indian Journal of Science and Technology, 2009. **2**(10): p. 44-47.
11. Mujumdar, A., *CLASSIFICATION AND SELECTION OF INDUSTRIAL DRYERS.* Exergex Corp., 2000.
12. Ogolla, J.A., et al., *Influence of Inlet Drying Air Temperature and Milk Flow Rate on the Physical, Optical and Thermal Properties of Spray-Dried Camel Milk Powders.* Food and Bioprocess Technology, 2019. **12**(5): p. 751-768.
13. Gouaou, I., et al., *Impact of operating conditions on a single droplet and spray drying of hydroxypropylated pea starch: Process performance and final powder properties.* Asia-Pacific Journal of Chemical Engineering, 2019. **14**(1): p. e2268.
14. Fox, B., G. Bellini, and L. Pellegrini, *Chapter 14 - Drying*, in *Fermentation and Biochemical Engineering Handbook (Third Edition)*, H.C. Vogel and C.M. Todaro, Editors. 2014, William Andrew Publishing: Boston. p. 283-305.
15. Mezhericher, M., A. Levy, and I. Borde, *Heat and mass transfer of single droplet/wet particle drying.* Chemical Engineering Science, 2008. **63**(1): p. 12-23.
16. Francia, V., et al., *Agglomeration in counter-current spray drying towers. Part A: Particle growth and the effect of nozzle height.* Powder Technology, 2016. **301**: p. 1330-1343.
17. Westergaard, V. and N. A/S, *Milk Powder Technology: Evaporation and Spray Drying*. 2004: Niro A/S.
18. Adhikari, B., et al., *Stickiness in Foods: A Review of Mechanisms and Test Methods.* International Journal of Food Properties, 2001. **4**.
19. Muzaffar, K., G. Nayik, and P. Kumar, *Stickiness Problem Associated with Spray Drying of Sugar and Acid Rich Foods: A Mini Review.* Food and Nutrition Sciences, 2015. **s12**.
20. Vuataz, G., *The phase diagram of milk: a new tool for optimising the drying process.* Le lait, 2002. **82**(4): p. 485-500.
21. Birchal, V.S., et al., *Effect of Spray-Dryer Operating Variables on the Whole Milk Powder Quality.* Drying Technology, 2005. **23**(3): p. 611-636.
22. Rao, R.H. and P.M. Gupta, *Development of spray dried orange juice blended skim milk powder.* Le Lait, 2002. **82**(4): p. 523-529.
23. Martens, R. and M. Naudts, *The influence of the dry matter content, the homogenization and the heating of concentrate on physical characteristics of whole milk powder.* Milchwissenschaft, 1979.

24. Piatkowski, M. and I. Zbicinski, *Analysis of the Mechanism of Counter-current Spray Drying.* Transport in Porous Media, 2007. **66**(1): p. 89-101.
25. Cheng, F., X. Zhou, and Y. Liu. *Methods for improvement of the thermal efficiency during spray drying*. in *E3S Web of Conferences*. 2018. EDP Sciences.
26. Telang, A.M. and B.N. Thorat, *Optimization of Process Parameters for Spray Drying of Fermented Soy Milk.* Drying Technology, 2010. **28**(12): p. 1445-1456.
27. Mezhericher, M., A. Levy, and I. Borde, *Three-Dimensional Spray-Drying Model Based on Comprehensive Formulation of Drying Kinetics.* Drying Technology, 2012. **30**(11-12): p. 1256-1273.
28. Crowe, C. and A. Mujumdar, *Advances in Drying*. 1980, Hemisphere Publishing Corpn. p. 63-99.
29. Kieviet, F. and P. Kerkhof, *Air flow, temperature and humidity patterns in a co-current spray dryer: modelling and measurements.* Drying Technology, 1997. **15**(6-8): p. 1763-1773.
30. Langrish, T.A. and I. Zbicinski, *The Effects of Air Inlet Geometry and Spray Cone Angle on the Wall Deposition Rate in Spray Dryers.* Chemical Engineering Research & Design, 1994. **72**(3): p. 420-430.
31. Huang, L., K. Kumar, and A.S. Mujumdar, *Use of Computational Fluid Dynamics to Evaluate Alternative Spray Dryer Chamber Configurations.* Drying Technology, 2003. **21**(3): p. 385-412.
32. Huang, L.X., K. Kumar, and A.S. Mujumdar, *A comparative study of a spray dryer with rotary disc atomizer and pressure nozzle using computational fluid dynamic simulations.* Chemical Engineering and Processing: Process Intensification, 2006. **45**(6): p. 461-470.
33. Nijdam, J.J. and T.A.G. Langrish, *An Investigation of Milk Powders Produced by a Laboratory-Scale Spray Dryer.* Drying Technology, 2005. **23**(5): p. 1043-1056.
34. Tran, T.T.H., M. Jaskulski, and E. Tsotsas, *Reduction of a model for single droplet drying and application to CFD of skim milk spray drying.* Drying Technology, 2017. **35**(13): p. 1571-1583.
35. Huang, L., K. Kumar, and A.S. Mujumdar, *A Parametric Study of the Gas Flow Patterns and Drying Performance of Co-current Spray Dryer: Results of a Computational Fluid Dynamics Study.* Drying Technology, 2003. **21**(6): p. 957-978.
36. Anandharamakrishnan, C., et al., *A study of particle histories during spray drying using computational fluid dynamic simulations.* Drying Technology, 2010. **28**(5): p. 566-576.
37. Maryam, S., R. Amir, and H. Mohammad Sadegh, *CFD Modeling and Experimental Study of a Spray Dryer Performance.* Chemical Product and Process Modeling, 2014. **9**(1): p. 15-24.
38. Adhikari, B., et al., *Effect of addition of maltodextrin on drying kinetics and stickiness of sugar and acid-rich foods during convective drying: experiments and modelling.* Journal of Food Engineering, 2004. **62**(1): p. 53-68.
39. Farid, M., *A new approach to modelling of single droplet drying.* Chemical Engineering Science, 2003. **58**(13): p. 2985-2993.
40. Mikhailov, M.D., *Exact solution of temperature and moisture distributions in a porous half-space with moving evaporation front.* International Journal of Heat and Mass Transfer, 1975. **18**(6): p. 797-804.
41. Dalmaz, N., et al., *Heat and Mass Transfer Mechanisms in Drying of a Suspension Droplet: A New Computational Model.* Drying Technology, 2007. **25**(2): p. 391-400.
42. Chen, X.D., *Moisture Diffusivity in Food and Biological Materials.* Drying Technology, 2007. **25**(7-8): p. 1203-1213.
43. Patel, K., et al., *One-dimensional simulation of co-current, dairy spray drying systems - Pros and cons.* http://dx.doi.org/10.1051/dst/2009059, 2010. **90**.
44. Patel, K. and X. Chen, *Prediction of spray-dried product quality using two simple drying kinetics models.* Journal of Food Process Engineering, 2005. **28**: p. 567-594.
45. Chen, X.D. and G.Z. Xie, *Fingerprints of the Drying Behaviour of Particulate or Thin Layer Food Materials Established Using a Reaction Engineering Model.* Food and Bioproducts Processing, 1997. **75**(4): p. 213-222.

46. Chen, X.D. and S.X.Q. Lin, *Air drying of milk droplet under constant and time-dependent conditions.* AIChE Journal, 2005. **51**(6): p. 1790-1799.
47. Pawar, S., et al. *Drying kinetics of droplets containing solids using reaction engineering approach*. in *International Drying Symposium. France*. 2014.
48. Chen, X.D., *The basics of a reaction engineering approach to modeling air-drying of small droplets or thin-layer materials.* Drying Technology, 2008. **26**(6): p. 627-639.
49. Fu, N., et al., *Reaction Engineering Approach (REA) to model the drying kinetics of droplets with different initial sizes—experiments and analyses.* Chemical Engineering Science - CHEM ENG SCI, 2011. **66**: p. 1738-1747.
50. Jin, Y. and X. Chen, *Numerical Study of the Drying Process of Different Sized Particles in an Industrial-Scale Spray Dryer.* Drying Technology, 2009. **27**: p. 371-381.
51. Jin, Y. and X.D. Chen, *A Three-Dimensional Numerical Study of the Gas/Particle Interactions in an Industrial-Scale Spray Dryer for Milk Powder Production.* Drying Technology, 2009. **27**(10): p. 1018-1027.
52. *ANSYS documentation - DPM boundary types*. Available from: https://www.afs.enea.it/project/neptunius/docs/fluent/html/ug/node699.htm.
53. Kashinath, K. and L. Tim, *Prediction of Deposition Patterns in a Pilot-Scale Spray Dryer Using Computational Fluid Dynamics (CFD) Simulations.* Chemical Product and Process Modeling, 2007. **2**(3).
54. Kota, K. and T.A.G. Langrish, *Prediction of wall deposition behaviour in a pilot-scale spray dryer using deposition correlations for pipe flows.* Journal of Zhejiang University-SCIENCE A, 2007. **8**(2): p. 301-312.
55. Hennigs, C., T.K. Kockel, and T.A.G. Langrish, *NEW MEASUREMENTS OF THE STICKY BEHAVIOR OF SKIM MILK POWDER.* Drying Technology, 2001. **19**(3-4): p. 471-484.
56. Harvie, D.J.E., T.A.G. Langrish, and D.F. Fletcher, *A Computational Fluid Dynamics Study of a Tall-Form Spray Dryer.* Food and Bioproducts Processing, 2002. **80**(3): p. 163-175.
57. Jin, Y. and X.D. Chen, *A Fundamental Model of Particle Deposition Incorporated in CFD Simulations of an Industrial Milk Spray Dryer.* Drying Technology, 2010. **28**(8): p. 960-971.
58. Jubaer, H., et al., *On the effect of turbulence models on CFD simulations of a counter-current spray drying process.* Chemical Engineering Research and Design, 2019. **141**: p. 592-607.
59. Kuriakose, R. and C. Anandharamakrishnan, *Computational fluid dynamics (CFD) applications in spray drying of food products.* Trends in Food Science & Technology, 2010. **21**(8): p. 383-398.
60. *Turbulence models*. Available from: https://www.engineering.com/DesignSoftware/DesignSoftwareArticles/ArticleID/13743/Choosing-the-Right-Turbulence-Model-for-Your-CFD-Simulation.aspx.
61. Oakley, D.E. and R.E. Bahu, *Computational modelling of spray dryers.* Computers & Chemical Engineering, 1993. **17**: p. S493-S498.
62. Huang, L., K. Kumar, and A. Mujumdar, *Simulation of a spray dryer fitted with a rotary disk atomizer using a three-dimensional computional fluid dynamic model.* Drying Technology, 2004. **22**(6): p. 1489-1515.
63. Huang, L. and A.S. Mujumdar, *Simulation of an industrial spray dryer and prediction of off-design performance.* Drying technology, 2007. **25**(4): p. 703-714.
64. *Scalable wall function - ANSYS theory guide*. Available from: https://www.afs.enea.it/project/neptunius/docs/fluent/html/th/node99.htm.
65. *Standard K epsilon model*. ANSYS Fluent Theory Guide; Available from: https://www.afs.enea.it/project/neptunius/docs/fluent/html/th/node58.htm.
66. Patel, K. and X. Chen. *The reaction engineering approach to estimate surface properties of aqueous droplets during convective drying*. in *International Drying Symposium*. 2008.
67. Incropera, F.P., et al., *Fundamentals of heat and mass transfer, John Wiley & Sons.* Inc., Hoboken, NJ., 981p, 2002.

68. Qi Lin, S.X. and X.D. Chen, *Improving the Glass-Filament Method for Accurate Measurement of Drying Kinetics of Liquid Droplets.* Chemical Engineering Research and Design, 2002. **80**(4): p. 401-410.
69. Afshar, S., et al., *A practical CFD modeling approach to estimate outlet boundary conditions of industrial multistage spray dryers: Inert particle flow field investigation.* Drying Technology, 2019. **37**(7): p. 824-838.
70. Woo, M.W., et al., *CFD evaluation of droplet drying models in a spray dryer fitted with a rotary atomizer.* Drying Technology, 2008. **26**(10): p. 1180-1198.
71. Ozmen, L. and T.A.G. Langrish, *COMPARISON OF GLASS TRANSITION TEMPERATURE AND STICKY POINT TEMPERATURE FOR SKIM MILK POWDER.* Drying Technology, 2002. **20**(6): p. 1177-1192.
72. Chandan, R.C. and A. Kilara, *Dairy-Based Ingredients.* Dairy Processing and Quality Assurance, 2015: p. 197.

APPENDIX

A. Mesh Independence study

Mesh independence of results was determined by comparing the velocity profile along vertical axis, velocity and pressure at the outlet.

Mesh Size (mm)	Nodes	Elements
0.5	249915	1338614
0.45	322829	1738519
0.4	424645	2296093
0.38	494512	2629943
0.35	599331	3265755
0.32	755204	4133501

Table.6

The element size was gradually decreased from 0.5cm and corresponding outlet parameters are checked for consistency.

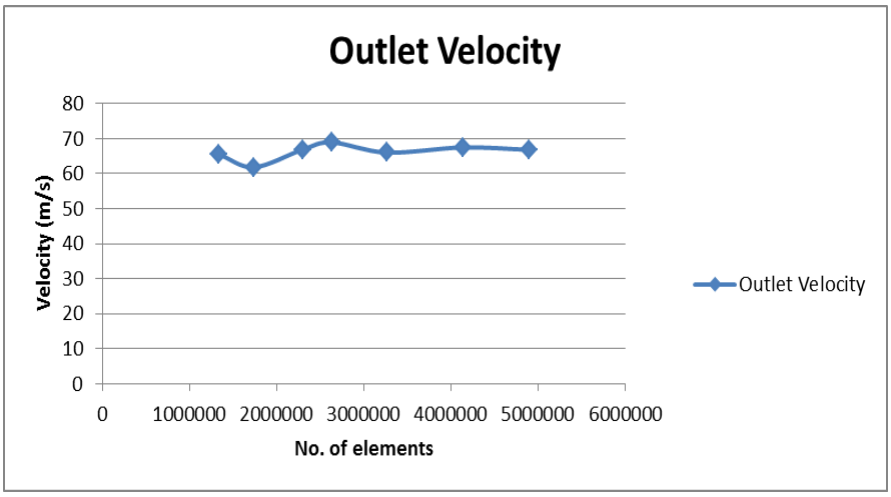

Fig.42

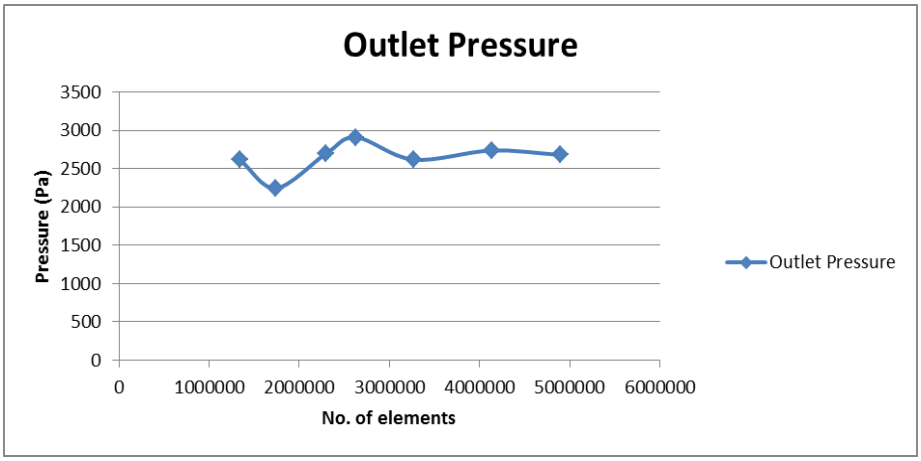

Fig.43

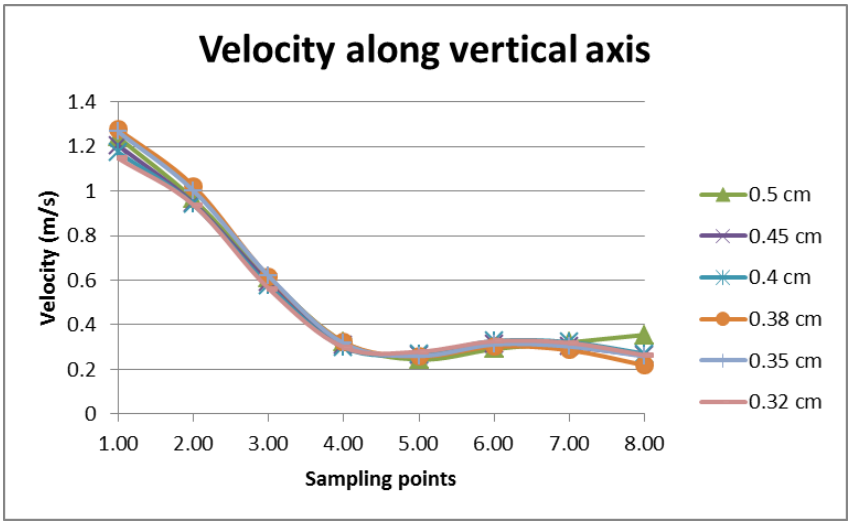

Fig.44

From the above graphs, it is evident that from 3.2M elements / 0.35cm the results are consistent with very slight deviation. The mesh quality is examined by orthogonal quality and skewness. For 0.35 cm element size, orthogonal quality has a minimum of 0.25723 and maximum of 0.99701 which is much above the worst case of zero. The skewness value has a minimum of 1.02E-06 and maximum of 0.74277 which are significantly lower than the worst case of 1. Therefore an element size of 0.35cm is chosen for the mesh independence results and it is used throughout the study.

B. Droplet size data

The experimental data measured above 2cm from nozzle inlet for 0.5mm orifice diameter nozzle, is extrapolated for 49.4 bar pressure and used in this study. The experimental data are as follows

Viscosity: 1cP (Water)				Viscosity: 5cP (Milk)			
Pressure(bar)	SMD(µm)	D90(µm)	D10(µm)	Pressure(bar)	SMD(µm)	D90(µm)	D10(µm)
10	62.6	124.2	32.8	10	73.4	162.3	34.3
20	56.2	109.5	30.6	20	62.3	133.6	31.2
30	52.5	103.8	28.9	30	55.4	111.2	29.2

With the nozzle calibration equation, it is found that 21.5 kg/hr corresponds to pressure of 49.4 bar. Therefore the experimental data is extrapolated based on the decreasing rate of change for diameters with consecutive increase in pressure. This method gave more realistic values compared to curve fitting, with the constraint that diameter of milk droplets is always greater than that of water.

Viscosity: 1cP (Water)				Viscosity: 5cP (Milk)			
Pressure(bar)	SMD(µm)	D90(µm)	D10(µm)	Pressure(bar)	SMD(µm)	D90(µm)	D10(µm)
49.4	49.8	95.19	27.38	49.4	50.2	98.5	27.5

C. Nozzle calibration

The hollow cone nozzle with orifice diameter of 0.5mm is calibrated for mass flow rate, before the use in experiment.

Signal	Pressure (bar)	Mass difference(g)	Time(s)	Flow rate (kg/hr)
0.008	13.8	13.792	90	11.596
0.01	31.3	31.29	90	16.968
0.012	49	48.988	90	21.596
0.0123	52	51.9877	90	21.968
0.014	60.5	60.486	90	23.88

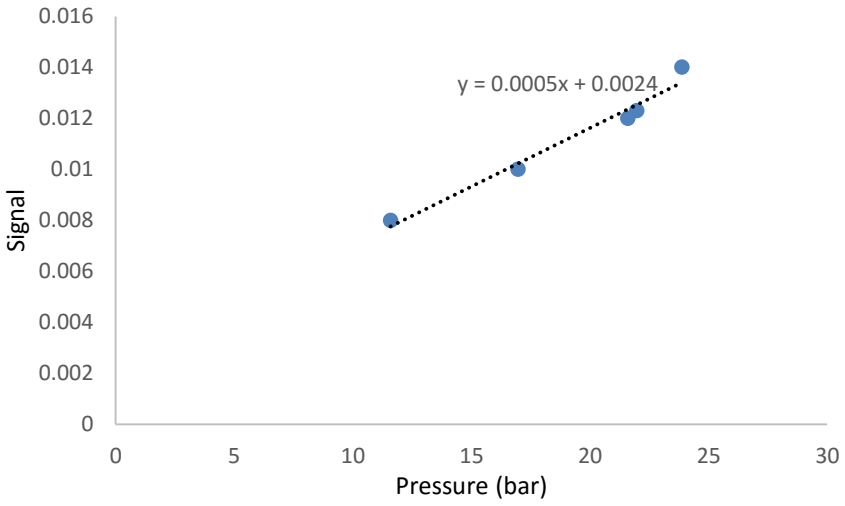

Fig.45

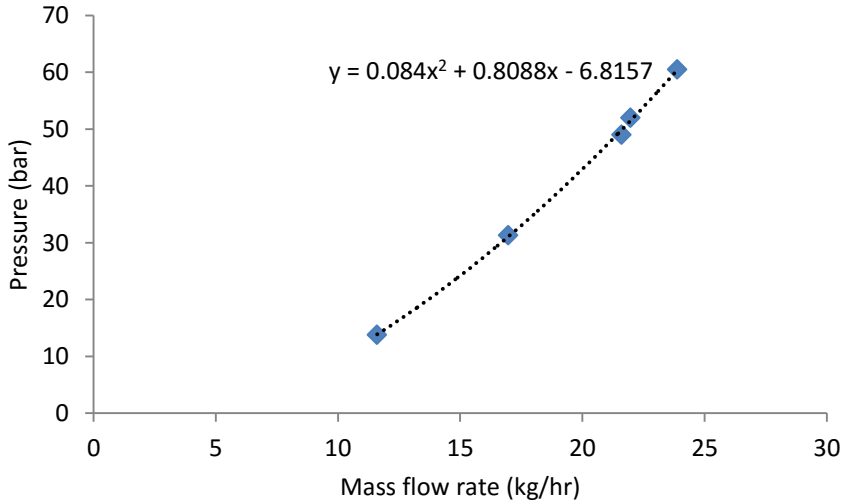

Fig.46

The above equations are used for signal input for nozzle based on flow rate in the experiments. They are also used in the calculation of pressure for the provided mass flow rates.

D. UDFs

The macros are defined in the ANSYS Fluent UDF manual. The REA model is implemented in FLUENT by using an UDF with macro DEFINE_DPM_VP_EQUILIB and hooked to equilibrium vapor concentration which in default is calculated using Raoults law. Diffusivity is defined through the macro DEFINE_DIFFUSIVITY, whereas drag co-efficient is modified using DEFINE_DPM_DRAG. The deposition model is implemented using the macros, DEFINE_DPM_BC, DEFINE_DPM_SOURCE and DEFINE_DPM_EROSION. DEFINE_DPM_BC is used to check whether the particle interacting with the wall is at sticky point temperature and a particle scalar is used to pass this information. If the particle is to be deposited, DEFINE_DPM_EROSION is used to update for the accretion rate. In two-way coupling, the continuous phase is updated when the particle crosses the cell boundary. DEFINE_DPM_SOURCE provides access to the accumulated source that is to be transferred to continuous phase. Therefore it is used to consider evaporation of water for the particles that stick to the wall. Once updated, the particle is removed from the domain.

```
#include "udf.h"

#include "dpm_mem.h"

DEFINE_DPM_VP_EQUILIB(rea,tp,Tp,cvap_surf,Z)
        {
        int is;  int ns;
        Material *sp; /*species pointer*/
        real molwt[MAX_SPE_EQNS];     /*creates an array of size => number of species*/
        Thread *t0 = TP_CELL_THREAD(tp);  /* cell thread of particle location */
        Material *gas_mix = THREAD_MATERIAL(t0); /* gas mixture material */
        Material *cond_mix = TP_MATERIAL(tp); /* particle mixture material */
        int nc = TP_N_COMPONENTS(tp);    /* number of particle components */
        real molwt_cond = 0.;  /* reciprocal molecular weight of the particle */
        real Xv =0; real molwt_bulk=0;
        real Xb =0; real free_moi =0;
        cphase_state_t *c = &(tp->cphase[0]); /* cell information of particle location*/
        int m = 0.06156; int k = 5.71*exp(-5118/UNIVERSAL_GAS_CONSTANT/c->temp);
         int d= 0.001645*exp(24831/UNIVERSAL_GAS_CONSTANT/c->temp);
        /*skim milk-GAB constants*/
        mixture_species_loop(gas_mix,sp,ns)
        {
```

```
molwt[ns] = MATERIAL_PROP(sp,PROP_mwi); /* molecular weight of gas species */

molwt_bulk += c->yi[ns] / molwt[ns]; /* yi is mass fraction ; reciprocal of average molecular weight */   }

          for (is = 0; is < nc; is++)

{

int gas_index = TP_COMPONENT_INDEX_I(tp,is); /* index of vaporizing component in the gas phase */

if (gas_index >= 0)   /*returns -1 for non-vap species*/

{

  /* the molecular weight of particle material */

molwt[gas_index=MATERIAL_PROP(MIXTURE_COMPONENT(gas_mix,gas_index),PROP_mwi);

Xv += TP_COMPONENT_I(tp,is)/(1-TP_COMPONENT_I(tp,is));

 /* particle surface moisture content -Ref: REA to estimate surf */

molwt_cond += TP_COMPONENT_I(tp,is) / molwt[gas_index];

 /*reciprocal of avg mol.wt of condensed state*/

 }      }

real  psat_bulk = pow(10,(7.94917-(1657.462/(c->temp - 46.23))))*133.322;

/* prevent division by zero */

molwt_cond = MAX(molwt_cond,DPM_SMALL);

for (is = 0; is < nc; is++)  {

/* gas species index of vaporization */

int gas_index = TP_COMPONENT_INDEX_I(tp,is);

if(gas_index >= 0)  {

/* condensed material */

Material * cond_c = MIXTURE_COMPONENT(cond_mix, is);

/* condensed component molefraction */

real xi_cond = TP_COMPONENT_I(tp,is)/(molwt[gas_index]*molwt_cond);

real cvap_bulk = c->pressure / UNIVERSAL_GAS_CONSTANT / c->temp * c->yi[gas_index] / molwt_bulk/ solver_par.molWeight[gas_index];
```

```
/*mole fraction of evap species is multiplied*/

real csat_bulk =  psat_bulk/ UNIVERSAL_GAS_CONSTANT / c->temp;

/*real p_saturation = pow(10,(7.94917-(1657.462/(Tp - 46.23))))*133.322;

Antoine's equation - ref: REA to estimate surface prop of aqueous droplets*/

real csat_surf = (4.844*pow(10,-9)*pow((Tp-273),4))-(1.4807*pow(10,-7)*pow((Tp-273),3))+(2.6572*pow(10,-5)*pow((Tp-273),2))-(4.8613*pow(10,-5)*(Tp-273))
+(8.342*pow(10,-3));     /*mass concentration*/

csat_surf=csat_surf/molwt[gas_index]; /*converting to molar concentration*/

int aw = xi_cond;

Xb = (m*k*d*aw)/((1-k*aw)*(1-k*aw+d*k*aw));

free_moi = Xv-Xb;

real del_Evb = -UNIVERSAL_GAS_CONSTANT  * (c->temp)  * log(cvap_bulk/csat_bulk);

real ax = ((-6.47438*pow(10,-3)*pow(free_moi,5)) + (8.86858*pow(10,-2)*pow(free_moi,4)) -
(0.471097*pow(free_moi,3)) + (1.22317*pow(free_moi,2)) +(-1.62539*free_moi) + (1.0092));
/*HAL*/

real del_Ev = ax*del_Evb;

/*fractionality co-efficient- relative humidity at the interface of the particle-particle and the drying air(REA)*/

real fr_co = exp(-del_Ev/UNIVERSAL_GAS_CONSTANT / Tp);

    for (is = 0; is < nc; is++)     {

int gas_index = TP_COMPONENT_INDEX_I(tp,is); /* index of vaporizing component in the gas phase */

if (gas_index >= 0)   /*returns -1 for non-vap species*/

{

if(TP_COMPONENT_I(tp,gas_index)<0.0000001) {

cvap_surf[is] = cvap_bulk ;}

else{

cvap_surf[is] = fr_co * p_saturation / UNIVERSAL_GAS_CONSTANT / Tp;  }

 }   }  }}

/* compressibility for ideal gas */  *Z = 1.0; }
```

```
DEFINE_DIFFUSIVITY(air_vapor_mixture_diffusivity,c,t,i) /* air-vapor mixture diffusivity*/
        {
        real temp=C_T(c,t);
        real Dv = (1.963*pow(10,-7)*temp)-3.33307*pow(10,-5); /*Incropera F.P., DeWitt D.P., Fundamentals of Heat and Mass Transfer*/
        return Dv;
        }
DEFINE_DPM_DRAG(particle_drag_force,Re,tp) {
        return(0);
        }
DEFINE_DPM_BC(bc_reflect,tp,t,f,f_normal,dim)
{
real alpha; /* angle of particle path with face normal */
real vn=0.;  real ms; real wm; real p =0; real tg = 0; real cr= 0; int is;
int nc = TP_N_COMPONENTS(tp);
real nor_coeff =0; real tan_coeff =0;
for (is = 0; is < nc; is++)
        {
        int gas_index = TP_COMPONENT_INDEX_I(tp,is); /* index of vaporizing component in the gas phase */
        if (gas_index >= 0)   /*returns -1 for non-vap species*/
        {
        wm=TP_COMPONENT_I(tp,gas_index);
        ms = 1-wm;
        p =wm*7.4;
        tg = ((101*ms-135*p)/(ms+p));
        tg=tg+273;
/* resitution coefficent */
nor_coeff =1;
```

```
tan_coeff =1;
/* diff bw glass transition and sticky point */
if(TP_T(tp) - tg >= 23.3 )
{
TP_COMPONENT_I(tp,gas_index) =0;
TP_USER_REAL(tp,0)=1;
}}}
real normal[3];    int i; int idim = dim;    real NV_VEC(x);
 #if RP_2D
/* dim is always 2 in 2D compilation. Need special treatment for 2d axisymmetric and swirl flows */
if (rp_axi_swirl)     {
real R = sqrt(TP_POS(tp)[1]*TP_POS(tp)[1] + TP_POS(tp)[2]*TP_POS(tp)[2]);
if (R > 1.e-20)          {
idim = 3;
normal[0] = f_normal[0];
normal[1] = (f_normal[1]*TP_POS(tp)[1])/R;
normal[2] = (f_normal[1]*TP_POS(tp)[2])/R;
 }
else
{             for (i=0; i<idim; i++)
             normal[i] = f_normal[i];          }       }
else
#endif
for (i=0; i<idim; i++)
normal[i] = f_normal[i];
if(TP_TYPE(tp) == DPM_TYPE_MULTICOMPONENT)
{
```

```
alpha = M_PI/2. - acos(MAX(-1.,MIN(1.,NV_DOT(normal,TP_VEL(tp))/
MAX(NV_MAG(TP_VEL(tp)),DPM_SMALL))));

if ((NNULLP(t)) && (THREAD_TYPE(t) == THREAD_F_WALL))

F_CENTROID(x,f,t);

      /* calculate the normal component, rescale its magnitude by  the coefficient of restitution and
subtract the change */

      /* Compute normal velocity. */

for(i=0; i<idim; i++)

vn += TP_VEL(tp)[i]*normal[i];

      /* Subtract off normal velocity. */

for(i=0; i<idim; i++)

TP_VEL(tp)[i] -= vn*normal[i];

      /* Apply tangential coefficient of restitution. */

for(i=0; i<idim; i++)

TP_VEL(tp)[i] *= tan_coeff;

      /* Add reflected normal velocity. */

for(i=0; i<idim; i++)

TP_VEL(tp)[i] -= nor_coeff*vn*normal[i];

      /* Store new velocity in TP_VEL0 of particle */

for(i=0; i<idim; i++)

TP_VEL0(tp)[i] = TP_VEL(tp)[i];

           return PATH_ACTIVE;     }

  return PATH_ABORT; }


DEFINE_DPM_EROSION(dpm_accr, tp, t, f, normal, alpha, Vmag, Mdot)

{

real A[ND_ND], area;  int is; int nc = TP_N_COMPONENTS(tp); real ms;

real wm; real p =0; real tg = 0;

 for (is = 0; is < nc; is++)
```

```
        {
        int gas_index = TP_COMPONENT_INDEX_I(tp,is); /* index of vaporizing component in the gas phase */
        if (gas_index >= 0)   /*returns -1 for non-vap species*/
        {
wm=TP_COMPONENT_I(tp,gas_index);
ms = 1-wm;
p =wm*7.4;
tg = ((101*ms-135*p)/(ms+p));
tg=tg+273;
if(TP_T(tp) - tg < 23.3 )
return;
F_AREA(A,f,t);
area = NV_MAG(A);
F_STORAGE_R(f,t,SV_DPMS_ACCRETION) += (1-TP_COMPONENT_I(tp,gas_index)) *Mdot / area;}}}
 DEFINE_DPM_SOURCE(dpm_source, c, t, S, strength, tp)
 {
real mp_dot;
 Material *m = THREAD_MATERIAL(t);
int i = mixture_specie_index(m, "h2o");
mp_dot =  (TP_MASS0(tp) - TP_MASS(tp)) * strength;
S->species[i] += mp_dot;
S->energy -= mp_dot * 2263073;
if (TP_USER_REAL(tp,0)== 1)    {
MARK_TP(tp, P_FL_REMOVED);
 } }
```

E. Cross sectional comparison of temperature profiles

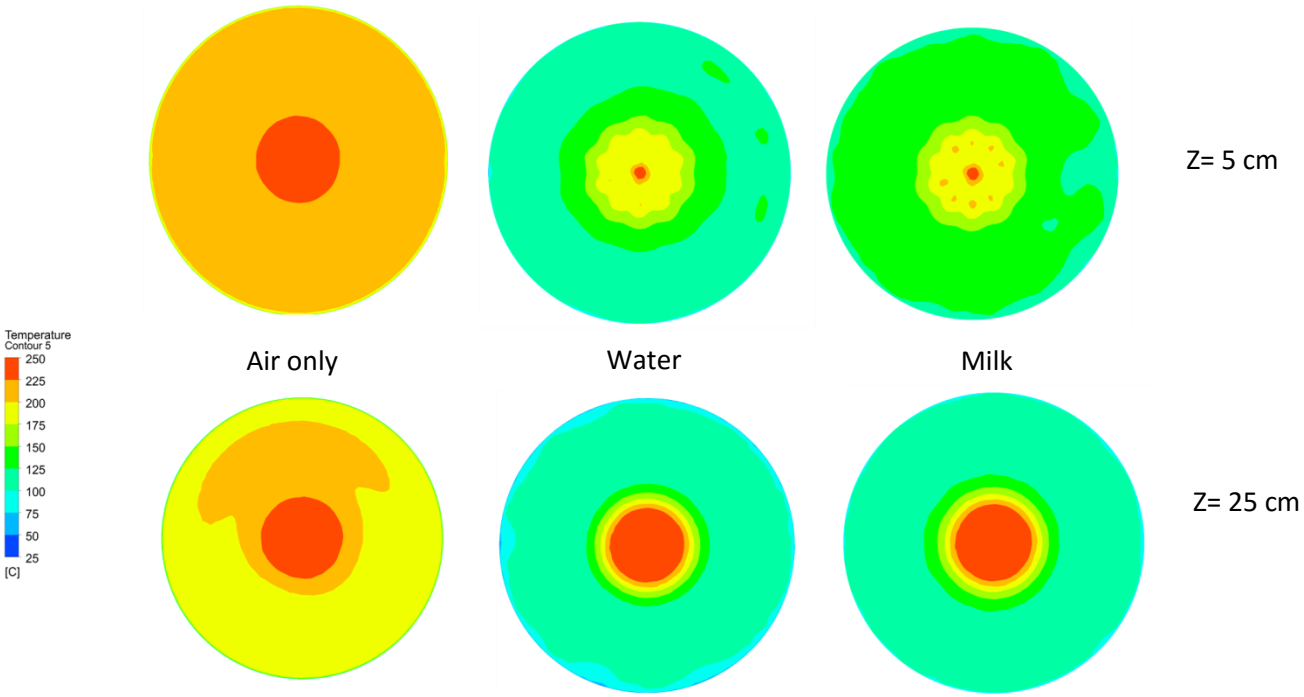

Fig.47